Extratropical Sub-seasonal to Seasonal Oscillations and Multiple Regimes: The Dynamical Systems View

Michael Ghil, Andreas Groth, Dmitri D Kondrashov, Andrew W Robertson

The following article appeared as chapter 6 in the book

Sub-Seasonal to Seasonal Prediction: The Gap Between Weather and Climate Forecasting
Elsevier, 2019, 585 pages.

https://doi.org/10.1016/B978-0-12-811714-9.00006-1

Extratropical sub-seasonal–to–seasonal oscillations and multiple regimes: The dynamical systems view

Michael Ghil[a,b,*], Andreas Groth[a], Dmitri Kondrashov[a], Andrew W. Robertson[c]

[a] *Department of Atmospheric and Oceanic Sciences, University of California at Los Angeles, Los Angeles, California*

[b] *Geosciences Department and Laboratoire de Météorologie Dynamique (CNRS and IPSL), Ecole Normale Supérieure and PSL Research University, Paris, France*

[c] *International Research Institute for Climate and Society (IRI), Columbia University, Palisades, New York*

Abstract

This chapter considers the sub-seasonal–to–seasonal (S2S) prediction problem as intrinsically more difficult than either short-range weather prediction or interannual–to–multidecadal climate prediction. The difficulty arises from the comparable importance of atmospheric initial states and of parameter values in determining the atmospheric evolution on the S2S time scale.

The chapter relies on the theoretical framework of dynamical systems and the practical tools this framework helps provide to low-order modeling and prediction of S2S variability. The emphasis is on mid-latitude variability and the complementarity of the nonlinear-waves vs. multiple-regime points of view in understanding this variability. Empirical model reduction and the forecast skill of the models thus produced in real-time prediction are reviewed.

Keywords: bifurcations, cluster analysis, empirical model reduction, hierarchy of models, singular spectrum analysis, predictability

Contents

*Corresponding author
Email address: ghil@atmos.ucla.edu (Michael Ghil)

1. Introduction and motivation

The John von Neumann point of view (Von Neumann, 1955): short-term numerical weather prediction (NWP) is the easiest — i.e., it is a pure initial-value problem; long-term climate prediction is next easiest — it corresponds to studying the system's asymptotic behavior; intermediate-term prediction is hardest — both initial & boundary values are important. The modeling hierarchy & successive bifurcations as Ariadne's thread through the rungs of the hierarchy.

Intraseasonal time scales, more recently called subseasonal-to-seasonal (S2S), range from the deterministic limit of atmospheric predictability, of about 10 days, up to a season, say 100 days. These time scales occupy a window of overlap between low-frequency variability (LFV) intrinsic to the atmosphere and short climatic time scales that also involve the upper ocean and land-surface features, as well as the stratosphere. These time scales are of particular importance to subseasonal prediction. Theoretical and observational studies of LFV over the past half-century have used two complementary ways of describing atmospheric LFV in the extratropics: (i) episodic, by means of multiple weather (Reinhold and Pierrehumbert, 1982) or flow (Charney and DeVore, 1979; Legras and Ghil, 1985) regimes; and (ii) oscillatory, by means of broad-peak, slowly modulated oscillations (Ghil and Robertson, 2002, and references therein).

We pursue throughout the chapter the dynamical systems point of view first formulated by John von Neumann (Von Neumann, 1955), according to which there are three levels of difficulty in understanding and predicting atmospheric phenomena: (a) short-term numerical weather prediction (NWP) is the easiest, since it represents a pure initial-value problem, as formulated by V. Bjerkness (Bjerknes, 1904) and L. F. Richardson (Richardson, 1922); (b) long-term climate prediction is next easiest, since it corresponds to studying the system's asymptotic behavior, i.e., the possible attractors — such as fixed points, limit cycles, strange attractors — and the statistical properties thereof (Ghil and Childress, 1987; Dijkstra and Ghil, 2005; Dijkstra, 2013); and (c) intermediate-term prediction is hardest, since both the initial and the parameter values are important. We deal with the latter problem by pursuing a full hierarchy of models, from the simplest to the most detailed ones (Schneider and Dickinson, 1974; Held, 2005), and the tool of successive bifurcations as Ariadne's thread through the rungs of this hierarchy (Ghil and Robertson, 2000; Ghil, 2001).

This chapter starts in Sec. 2 with a brief summary of the main characteristics of the oscillatory vs. intermittent viewpoints from a dynamical systems perspective, based on the review article of Ghil and Robertson (2002) and updated using studies published since then. Section 3 then presents a new analysis of the observational characteristics of oscillatory LFV, using a recently developed multivariate spectral analysis tool. With this background and results in hand, Sec. 4 discusses low-order modeling (LOM) approaches and their application to LFV, while outlining how these approaches have developed over the years from so-called linear inverse models (LIMs) or principal oscillation patterns (POPs) to empirical model reduction (EMR) and multi-level stochastic models (MSMs). The chapter concludes in Sec. 5 with the prospects for improving S2S prediction in the extratropics based on the theoretical LFV framework sketched herein and on data-driven LOMs.

2. Multiple mid-latitude regimes and low-frequency oscillations

Blocking, zonal flow, and teleconnection patterns; phenomenological description of extratropical flows in the S2S band (10–100 days). Mechanical- & thermal-topography effects, i.e., mountains & land–sea contrast. Bifurcations & symmetry breaking as the unifying point of view for the theoretical interpretation of the phenomenology. Markov chains of regimes & predictability.

2.1. The case for multiple regimes and their classification

Persistent LFV anomalies, in which the flow patterns differ significantly from the normal climatological circulation and remain stationary for more than a week, have been objectively identified over the North Pacific and North Atlantic in the 1980s (Wallace and Gutzler, 1981; Dole and Gordon, 1983; Mo and Ghil, 1988). Their onsets and breaks, on the other hand, are rather abrupt. The most familiar of these persistent patterns or "Grosswetterlagen" (Namias, 1968), albeit not the only ones, are blocked and zonal flows.

Within the last few decades it has been demonstrated that these patterns can be identified by examining the probability distribution function (pdf) of the corresponding large-scale maps in the atmosphere's phase space (Cheng and Wallace, 1993; Kimoto and Ghil, 1993a,b; Smyth et al., 1999). The resulting patterns resemble those found previously by using correlation analysis.

Many of the methods used to classify weather maps are summarized in Table 1. In such a classification, an individual atmospheric map is thought of as a point in phase space. To achieve a reliable, statistically significant classification, it is necessary to consider a low-dimensional subspace of this phase space that still captures most of the variance in the data set. The usual choice is to compute the analyzed record's empirical orthogonal functions (EOFs), i.e., the eigenvectors of the covariance (or correlation) matrix, and to select a subspace spanned by a few leading eigenvectors (Mo and Ghil, 1988; Cheng and Wallace, 1993; Kimoto and Ghil, 1993a,b; Smyth et al., 1999).

Many of the classification methods define the regimes as classes of distinct atmospheric states that have a high probability of occurrence and are separated by regions of lower probability. Some of these methods seek maxima of the pdf by using kernel density estimation (Kimoto and Ghil, 1993b; Corti et al., 1999) or more ad hoc methods (Molteni et al., 1990). Each regime is then formed by the points, or maps, that exceed a given probability threshold in the neighborhood of a pdf maximum. The number of pdf peaks depends on the kernel smoothing parameter used, which can be determined objectively by using a least-squares cross-validation procedure (Silverman, 1986).

Smyth et al. (1999) have used a mixture model that approximates the pdf by the sum of a small number of multivariate Gaussians. In this case, the regimes are "fuzzy" in the sense that they overlap, and that each particular daily weather map can be assigned a probability of belonging to one or another regime. This was the case also in Mo and Ghil (1988), who used a different classification algorithm, and obtained therewith a different number of regimes. This number, as well as the spatial patterns associated with the regimes, are discussed in Sec. 4.

Cluster analysis is a less ambitious approach to classifying atmospheric states: it localizes high concentrations of points, called clusters, but does not pretend to estimate the pdf. There are two main types of clustering algorithm: hierarchical and partitioning. In hierarchical algorithms, one builds a classification tree iteratively, starting from single data points and merging them into clusters according to a similarity criterion. Cheng and Wallace (1993) used Ward's method to do this. In partitioning algorithms, a prescribed number of clusters is chosen, and data points are agglomerated around kernels initially picked as random seeds. The kernels are iteratively modified so as to globally minimize the data scatter about them, as done in the K-means method of Michelangeli et al. (1995).

Using low-pass filtered data, based on running means of 5–10 days, introduces some measure of persistence into the above methods, which are based on frequency of occurrence. A second broad class of methods uses quasi-stationarity explicitly. Here, the regimes are defined as comprising states for which large-scale motion is slow in the statistical sense. More precisely, one seeks the large-scale patterns that have, on average, a small time derivative (Legras and Ghil, 1985). This phase-space speed can be computed for maps that do include synoptic-scale motions by a nonlinear equilibration technique (Vautard and Legras, 1988; Vautard, 1990; Michelangeli et al., 1995).

Huth et al. (2008) provided a more recent review of classification schemes of atmospheric circulation patterns, and included a table that updates the one of Ghil and Robertson (2002) reproduced herein. Straus et al. (2007) compared the circulation regimes in the National Center's for Environmental Prediction (NCEP's) reanalyses with the GCM model simulations of the Center for Ocean-Land-Atmosphere Studies (COLA), showing that three out of the four observed clusters have identifiable counterparts in the model simulations. These authors, as well as Straus and Molteni (2004), also studied possible changes in the structure of the COLA GCM's regimes in response to changes in tropical sea surface temperature (SST) forcing. Christensen et al. (2014), Dawson and Palmer (2014) and Muñoz et al. (2017) used weather regimes to evaluate more broadly the simulation skill of climate models, with Dawson and Palmer (2014), in particular, showing that higher horizontal resolutions in NWP models improves regime simulation.

Most recently, Hannachi et al. (2017) have reviewed the state of knowledge on the low-frequency fluctuations of the extratropical troposphere. These authors showed that retaining periods longer than 10 days yields statistically significant multiple regimes, while Stephenson et al. (2004), to the contrary, had found

Table 1: Classification methods for weather maps. Based on Ghil and Robertson (2002) and updated.

Approach	Method	Data sets	References	Comments
Regime classification by position				
Cluster analysis	Categorical	NH	Mo and Ghil (1988)	Fuzzy
		NH + sectorial	Michelangeli et al. (1995)	Hard (k-means)
		Model	Dawson and Palmer (2014)	Hard (k-means)
		Model+NH+sectorial	Muñoz et al. (2017)	Hard (k-means)
		Model + sectorial	Straus and Molteni (2004); Straus et al. (2007, 2017)	Hard (k-means)
	Hierarchical	NH + sectorial	Cheng and Wallace (1993)	3 NH clusters
PDF estimation	Univariate	NH	Benzi et al. (1986); Hansen and Sutera (1995)	Bimodality
	Multivariate	NH	Kimoto and Ghil (1993a)	3 modes
		NH + sectorial	Kimoto and Ghil (1993b); Smyth et al. (1999)	Multimodal 3 NH clusters
Regime classification by persistence				
Pattern correlations		NH	Horel (1985)	
		SH	Mo and Ghil (1987)	3 regimes
Minima of tendencies		Models	Legras and Ghil (1985); Mukougawa (1988); Vautard and Legras (1988)	
		Atl.-Eur. sector	Vautard (1990)	4 regimes
Transition probabilities				
Counts		Model + NH	Mo and Ghil (1988)	Elementary
Monte Carlo		NH + SH	Vautard et al. (1990)	Advanced
		NH + sectorial	Kimoto and Ghil (1993b)	Advanced

NH = Northern Hemisphere; SH = Southern Hemisphere; PDF = probability density function.

no strong evidence in monthly mean reanalysis data for rejecting the single-regime multinormal hypothesis. The obvious reason for the latter result seems to be that the number of maps retained by these authors was too small or that the subspace they retained was too large for a satisfactory estimation of the pdf. Another way of looking at the difference between the results of Hannachi et al. (2017) and of Stephenson et al. (2004) is the fact that the persistent anomalies associated with passage through the distinct regimes in phase space rarely lasts longer than ten days (Dole and Gordon, 1983; Kimoto and Ghil, 1993a,b). Thus, Hannachi et al. (2017) were separating such passages from the more diffuse flow in phase space outside the regimes, while Stephenson et al. (2004) were not.

Besides the fairly low degree of controversy that persists on the very existence of multiple regimes, there is still some lack of agreement as to their causes. Thus, Majda et al. (2006) find in a Hidden Markov Model (HMM) analysis that metastable regime transitions can occur despite a simple model's nearly Gaussian pdf, while Sura et al. (2005) show that deviations from Gaussianity can also result from linear, stochastically perturbed dynamics with multiplicative noise statistics. Deremble et al. (2012) show that thermal forcing by a time-independent SST front can affect the atmospheric flow patterns and bifurcation sequence obtained in atmospheric models with likewise time-independent, but mechanical, i.e. topographic forcing (Legras and Ghil, 1985; Jin and Ghil, 1990).

One may conclude that the number and variety of methods that have been used to identify and describe LFV regimes are leading up to a tentative consensus on their existence, robustness, and characteristics. We turn therewith to reviewing some of the theoretical foundations for the explanation of multiple regimes.

2.2. Theoretical basis of multiple regimes

Rossby wave propagation and interference. The slowly traveling, large-scale wave patterns that were first associated with weather phenomena in the 1930s are solutions of the partial differential equation for the conservation of potential vorticity q along a particle trajectory (Gill, 1982; Pedlosky, 1987). For the purposes of this expository review, q can be defined as the vorticity ζ of a column of fluid divided by its height h, i.e., $q = \zeta/h$. Conservation of q thus means, for instance, that a column of fluid's anti-clockwise rotation (defined as $\zeta > 0$) will slow down (i.e., ζ decreases to smaller positive values) as the column moves over a mountain range (i.e., $h > 0$ decreases). This type of vorticity balance leads to slow Rossby waves (Rossby et al., 1939; Haurwitz, 1940) that propagate westward with respect to the mean westerly jet. In this volume, Brunet and Methven (2018) present a more complete view of the role of such waves in S2S variability.

One view of persistent anomalies in mid-latitude atmospheric flows is that they result simply from the coincidental slowing down or linear interference of such Rossby waves (Lindzen et al., 1982; Lindzen, 1986). Another view is that a standing wave induced by topography can lead to a resonant interaction with two separate Rossby waves of distinct wavenumbers and thus produce a long-lived resonant wave triad (Egger, 1978; Ghil and Childress, 1987, Section 6.2). Neither one of these views provides an explanation of the observed clustering of persistent anomalies into distinct flow regimes. But the second one does suggest the more radically nonlinear theory described in the next few paragraphs.

Charney and DeVore (1979) took a major step in formulating a self-consistent atmospheric model for multiple equilibria and connecting it to observations of blocked and zonal flow. They used a highly idealized barotropic model to study the interaction between a zonal flow and simple topography with zonal wavenumber 2. Their model exhibits two stable equilibria for the same strength ψ_A^* of the prescribed zonal forcing that represents here the strength of the pole-to-equator temperature contrast. Charney et al. (1981) confronted the barotropic theory of Charney and DeVore (1979) with observations, while Charney and Straus (1980) extended it to baroclinic flows. In a somewhat complementary vein, Mitchell and Derome (1983) followed up on the suggestion (e.g., McWilliams, 1980, and references therein) that steady-state solutions of the inviscid potential vorticity equation, written as $q = G(\psi, p)$, can simulate blocking patterns, and may be resonantly excited by periodic forcing; here $\psi = \psi(x, y, p)$ is the stream function, p is pressure, and (x, y) are horizontal coordinates pointing east- and northward.

Figure 1 shows the Charney and DeVore (1979) model's bifurcation diagram, with the strength ψ_A of the zonal jet in the model's steady-state solutions plotted against the corresponding strength ψ_A^* of the forcing. The two stable equilibria—marked Z and R_-—are associated with "zonal" and "blocked" flow, respectively,

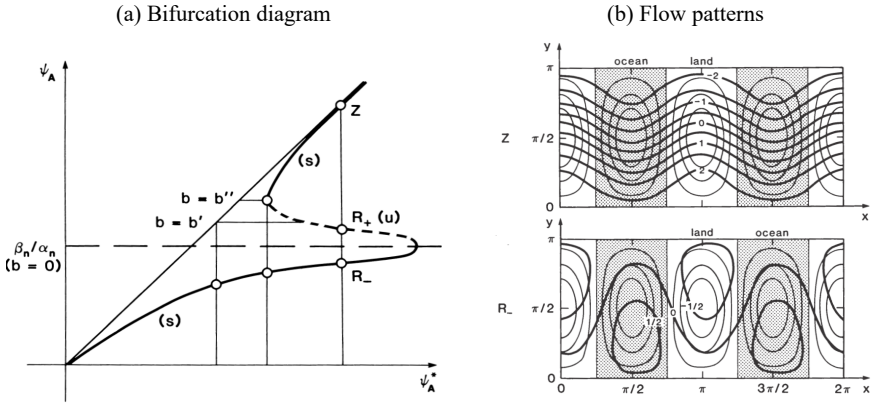

Figure 1: Multiple equilibria of a three-mode quasi-geostrophic model with simplified forcing and topography. (a) Bifurcation diagram showing model response to changes in forcing; see text for the explanation of abscissa and ordinate. The "S"-shaped bifurcation curve is typical of two back-to-back saddle-node bifurcations that give rise to two stable solution branches (solid) separated by an unstable one (dashed). (b) Flow patterns of the zonal (upper) and blocked (lower) branch, corresponding to the two stable equilibria Z and R$_-$ (after Charney and DeVore, 1979). (Reprinted with permission from Ghil and Childress (1987): Copyright 1987, Springer Nature.)

as illustrated in Fig. 1b. The near-zonal solution is close in amplitude and spatial pattern to the forcing jet and is influenced very little by the topography, whereas the blocked solution is strongly affected by it. In the blocked-flow solution, a high-amplitude ridge is located upstream of the "mountains," similar to the situation during typical observed blocks off the West Coast of North America. This configuration, with a negative zonal pressure gradient on the windward slope of the mountains, corresponds to a negative mountain torque on the atmosphere.

Benzi et al. (1986) and Hansen and Sutera (1995) found evidence of bimodality in a composite index of wave amplitude in the NH mid-latitude flow. Although the statistical significance and robustness of their findings have been subject to criticism (Nitsche et al., 1994), direct confrontation of theoretical bimodality with observations has clearly stimulated LFV research during the 1980s. Further comparisons between the various approaches to LFV and to S2S prediction are drawn in Sec. 5.

A reasonable classification of low-pass filtered flow maps into discrete regimes provides only a static view of LFV. The next step is to study the transitions between these regimes over time. A matrix of probabilities for transitions from regime i to regime j is constructed by simply counting the transitions occurring in the data set. This yields an estimated set of conditional probabilities, in line with long-range forecasting experience (Namias, 1968; Kalnay and Livezey, 1985) and the physical intuition that certain pathways of transition are more probable than others.

One kinematic approach to LFV is based on the Markov chain of these transitions. In this approach, knowledge of the system's present state is put to use to make a forecast, rather than using only unconditional probabilities. The Markov-chain view of LFV and, hence, long-range forecasting, is based on the existence of multiple regimes, the expected time of residence in each regime, and the probabilities of transition from one regime to another (Fig. 2).

Finally, several simple and intermediate model studies have addressed the issue of early warning indicators for regime transitions. For instance, Kondrashov et al. (2004) used the pdf of the exit angle from a given regime in a global baroclinic, quasi-geostrophic, 3-level (QG3) model with topography, originally due to Marshall and Molteni (1993), while Deloncle et al. (2007) used for the same model a fairly recent statistical learning method called random forests (Breiman, 2001). Kondrashov et al. (2007) then applied the random forests algorithm for studying regime transitions in Northern Hemisphere (NH) data sets, while Tantet et al. (2015) used transfer operator theory for the study of transitions from zonal to blocking events in a hemispheric barotropic model. Methods for the study and prediction of regime transitions are discussed in greater detail in Sec. 4.2, after having provided additional insight into LFV dynamics in Sec. 3.2.

3. Extratropical oscillations in the S2S band

Phenomenological description of the extratropical oscillations in the S2S band. Variations of atmospheric angular momentum (AAM). Topographic instability and Hopf bifurcation; transition to irregular, chaotic behavior. Extratropical oscillations in a GCM with no Madden-Julian Oscillation (MJO) in the tropics.

3.1. Phenomenological description

Variations of geopotential height. In this subsection, we analyze the geopotential height field at 500 hPa (Z500) from the ERA-interim reanalysis of Dee et al. (2011) that spans 37 years, January 1979–December 2016). We focus on the region $20°\mathrm{S} - 90°\mathrm{N}$, so as to include the tropics as well as the NH extratropics. This choice, along with that of the Z500 level, will become clearer as we proceed on to the results.

To identify spectral components of spatio-temporal behavior in the extensive ERA-interim reanalysis datasets, we apply here the multichannel singular spectrum analysis (M-SSA) methodology. For a comprehensive overview of the SSA and M-SSA methodology and of related literature, see Ghil et al. (2002) and (Alessio, 2016, chapter 12). M-SSA essentially diagonalizes the lag-covariance matrix of the multivariate dataset to yield a set of empirical orthogonal functions (EOFs) and the corresponding eigenvalues, which describe the variance captured by each EOF. In contrast to classical principal component analysis (PCA), M-SSA is able to capture oscillatory behavior in pairs of EOFs with approximately equal eigenvalues and dominant frequencies (Vautard and Ghil, 1989; Plaut and Vautard, 1994). To improve the separability of distinct frequencies, we rely here on a subsequent varimax rotation of the EOFs, cf. Groth and Ghil (2011).

Prior to the M-SSA analysis, the composite seasonal cycle is first subtracted from the daily time series. This cycle is computed by averaging the time series at each grid point over all years for each calendar day, and by smoothing this average using a 15-day running mean. Following Feliks et al. (2010, and references therein), we apply next a Chebyshev type I filter to the time series of anomaly maps, i.e., of the differences between the raw maps and the seasonal cycle so obtained, a lowpass filter that removes high-frequency oscillations with a period shorter than 20 days. The lowpass-filtered Z500 anomalies are subsampled with a sampling rate of 10 days, which yields time series of roughly 1300 samples. Finally, the subsampled anomalies are projected onto the 40 leading spatial EOFs of a classical PCA analysis, capturing 90% of the total variance. The corresponding principal components, finally, give the $D = 40$ input channels for the M-SSA analysis; see Groth et al. (2017) for further details of M-SSA analyzing extensive reanalysis datasets.

Oscillatory features in time and space. Figure 3(a) shows the eigenvalue spectrum of the subsampled Z500 anomalies. The spectrum exhibits several highly significant spectral peaks in the intraseasonal band; their

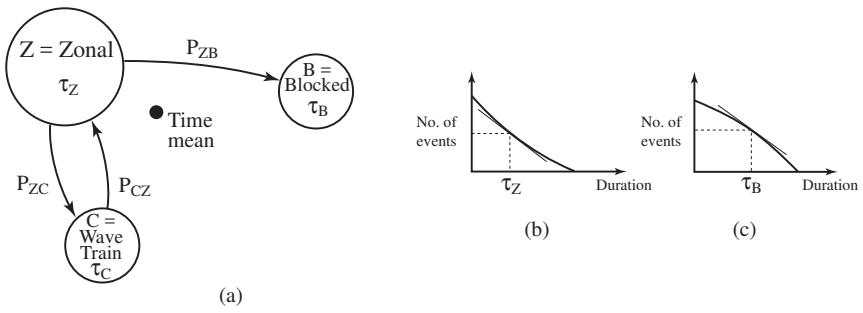

Figure 2: Schematic Markov chain with three regimes, B, C, and Z, for 'Blocked', 'Wave Train' and 'Zonal'. (a) Some preferential paths between pairs of regimes are shown, along with the corresponding transition probabilities, for instance p_{ZB} . (b and c) The distribution of residence times in log-linear coordinates differs from the straight line associated with a red-noise process; the mean residence time for each regime is denoted by τ. (Reprinted with permission from Ghil (1987): Copyright 1987, Springer Nature.)

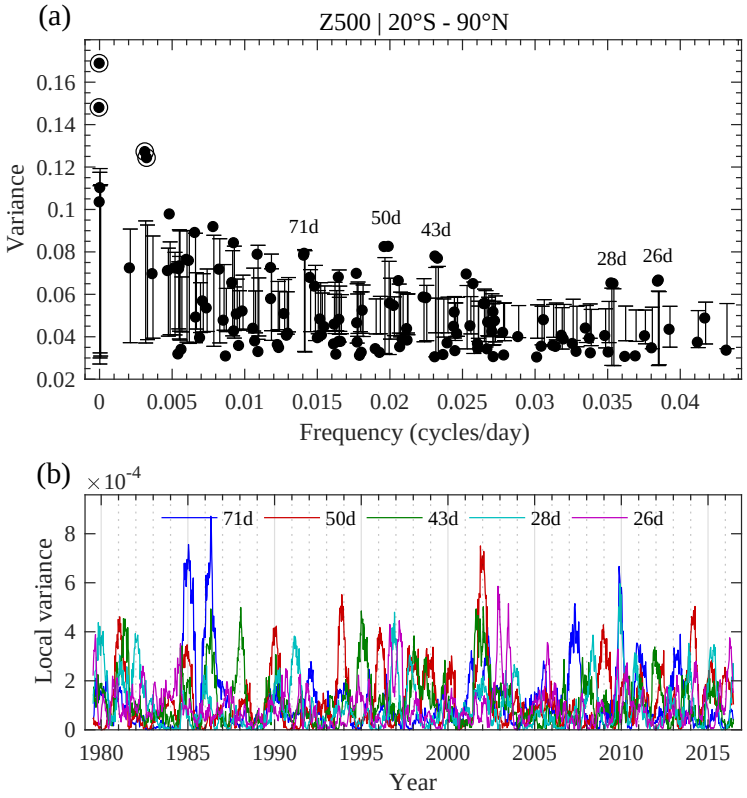

Figure 3: Intraseasonal oscillations of 500 hPa geopotential height (Z500) in the ERA-interim reanalysis for the time interval 1979–2016 and the region (20°S–90°N). (a) Spectrum of eigenvalues (black dots) plotted as a function of the associated dominant frequency from an M-SSA analysis with a window length of $M = 35$ (350 days); the subsequent varimax rotation uses EOFs 1–40. The corresponding period length (in days) for the key oscillatory pairs in the S2S band is indicated. Lower and upper limits of the error bars correspond to the 2.5% and 97.5% quantiles of a Monte Carlo test against the composite null hypothesis of EOFs 1–4 plus AR(1) noise; the test ensemble has 1000 members. EOFs 1–4 (target dots) correspond to the trend and to a peak that lies below the S2S range of interest herein. (b) Local variance captured by the oscillatory pairs that are indicated in the upper panel, as a function of time.

frequencies agree very well with those identified and described in detail in previous studies (Ghil and Mo, 1991; Plaut and Vautard, 1994). In particular, two eigenvalue pairs stand out clearly above the red-noise spectrum at periods of 50 and 43 days, along with two shorter-period oscillations at 28 and 26 days.

While Weickmann et al. (1985) discussed overall oscillatory behavior in the 30–60-day band, Dickey et al. (1991) showed that variations in global atmospheric angular momentum (AAM) exhibit spectral peaks with distinct periods near 40 and 50 days. The latter authors demonstrated that the 50-day peak is largely associated with AAM fluctuations in the Tropics, while the 40-day peak is associated primarily with variations in the strength of the mid-latitude westerlies, particularly in the NH. Indeed, the amplitude of the 40-day oscillation in zonal winds is known to be largest during boreal winter, when the winds are strongest in the NH (Weickmann et al., 1985; Ghil and Mo, 1991; Strong et al., 1993, 1995)

Our analysis of the Z500 anomalies goes into greater spatial detail than the zonally averaged one of Dickey et al. (1991). Herein, both oscillations, at 50 and at 43 days, make significant contributions to extratropical variability, with a Rossby wavetrain–like pattern across the North Atlantic extending into Eurasia, cf. Figs. 4(a,b). Figure 4(a), however, also shows a larger contribution of the 50-day oscillation to the dynamics in the Tropics, while a pattern that resembles the Pacific–North American (PNA) teleconnection extends northeastward from the Tropical Central Pacific; the 43-day oscillation, cf. Figure 4(b), is mainly limited to the NH, and contributes but little to the tropical LFV, except in the Atlantic sector.

Furthermore, the 28-day and 26-day oscillations that show up as significant in Fig. 3(a) have dynamical

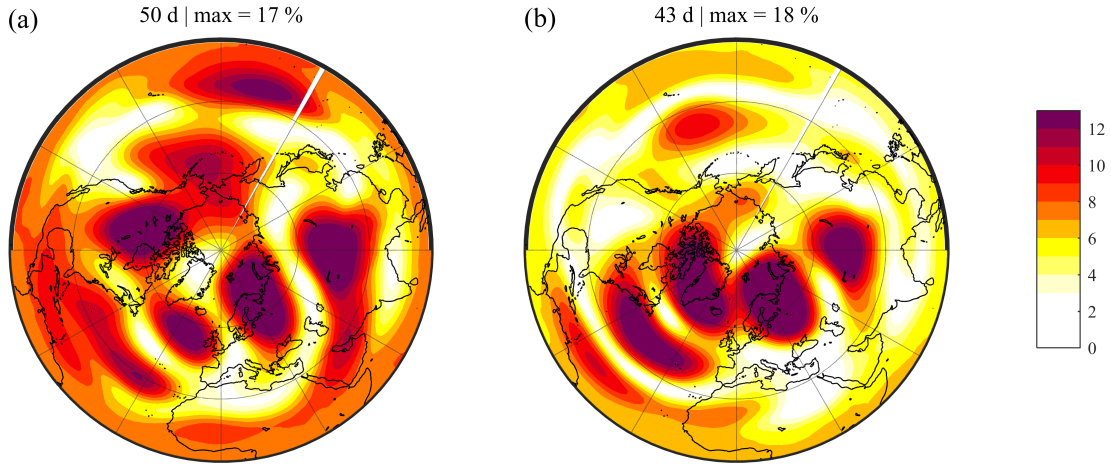

Figure 4: Spatial structure of intraseasonal Z500 variability with (a) periods of 50 days, and (b) of 43 days; based on the M-SSA analysis in Fig. 3. Shown is the relative standard deviation (in %) at each grid point, i.e. relative to the total standard deviation of overall Z500 variability.

patterns (not shown) that resemble a westward-traveling wave of this periodicity (Branstator, 1987; Kushnir, 1987; Dickey et al., 1991; Ghil and Mo, 1991). Figure 3(a) also points to a 71-day oscillation, whose period associates it with the 70-day oscillation emphasized by Plaut and Vautard (1994). The 71-day oscillation found in Z500 here, however, falls below the stringent 95% confidence level of the other four peaks.

To visualize the dynamics underlying the variability pattern in Figs. 4(a,b), we have also calculated phase composites of the 43-day and 50-day mode. The phase composites of the 43-day mode are shown in Fig. 5. This mode's spatio-temporal structure is characterized by a retroregressing wave train, and it bears a remarkable resemblence to the 30–35-day oscillation of Plaut and Vautard (1994). In phase category 1, we observe an amplification of the North Atlantic dipole structure, while in category 3, we observe a blocking pattern over Scandinavia. The overall pattern also shows greater variability in the Atlantic sector, with very little participation of the Pacific one.

The phase composites of the 50-day oscillation in Fig. 6 share certain features with the 43-day oscillations in the Atlantic sector, but exhibit much stronger variations in the Pacific sector. The 50-day tropical amplitude, although quite weak, suggests that the Pacific sector is much more involved in the tropical-extratropical interaction, whereas the 43-day mode in Fig. 5 is more focused on the Atlantic extratropical sector, in good agreement with the results of Plaut and Vautard (1994).

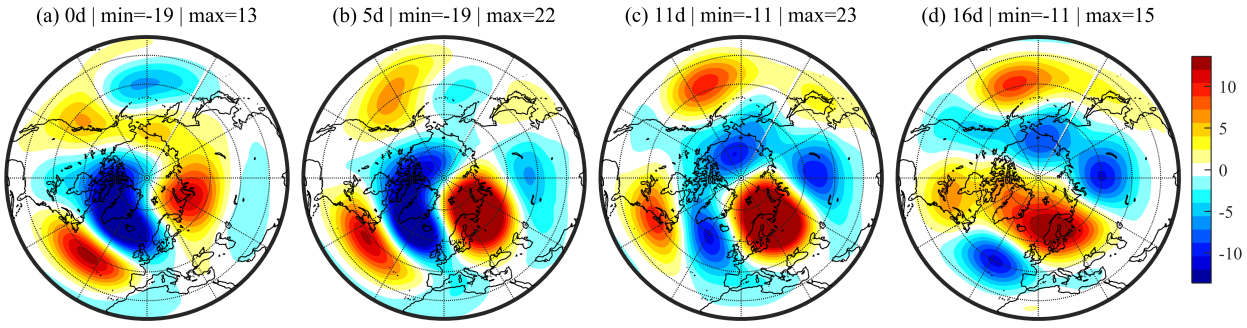

Figure 5: Phase composites of the 43-day oscillation from the M-SSA analysis of Z500 in Fig. 3. Four phases that correspond to one-half of the cycle are shown in color (in m). The phase categories are labeled in the panel legends by their midpoint (in days); also shown are the extreme values (min and max, in m).

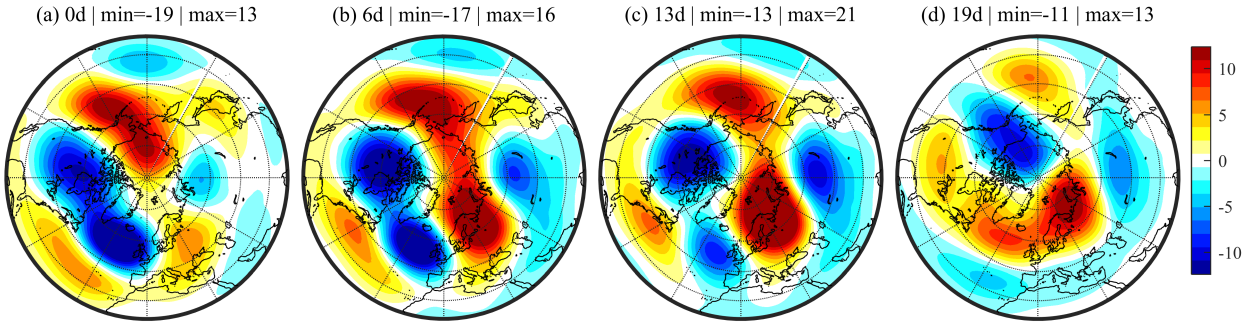

Figure 6: Same as Fig. 5, but showing the phase composites of the 50-day oscillation.

The present results thus concur, overall, with the conclusion of Plaut and Vautard (1994) that tropical-extratropical interactions in the intraseasonal band are much more active in the Pacific sector and with a 50-day periodicity, whereas the 43-day mode is more active in the Atlantic sector's extratropics. A similar distinction between the MJO and a separate 50-day mode in the Indian monsoon was made by Krishnamurthy and Achuthavarier (2012) and found to help S2S predictability there by Krishnamurthy and Sharma (2017). Even so, Cassou (2008) showed that the MJO does affect two of the four weather regimes defined by Vautard (1990) in the North Atlantic sector and Western Europe. Cassou's result is consistent, still, with Fig. 4, in which we observe a significant contribution of the 50-day oscillation in the NH.

In Fig. 3(b), we have furthermore calculated the local variance (Plaut and Vautard, 1994; Groth et al., 2015) for some of the intraseasonal oscillations, which shows a strong episodic modulation. This modulation illustrates one of the interesting relationships between the episodic, multiple-regime description of atmospheric LFV and the oscillatory one, based on intraseasonal oscillations (Kimoto and Ghil, 1993b; Plaut and Vautard, 1994; Koo et al., 2002; Crommelin, 2003, 2004; Kondrashov et al., 2004). The complementarity of these two points of view, episodic and oscillatory (Ghil and Robertson, 2002), will be discussed in Sec. 5.

3.2. Topographic instability and Hopf bifurcation

We outline here how a hierarchy of models (Ghil, 2001; Ghil and Robertson, 2000, 2002) can be used to formulate and test the hypothesis that the 40-day oscillation is an intrinsic mode of the NH extratropics, associated with the interaction between the jet stream and mid-latitude mountain ranges. The rudiments of this hypothesis originate in the highly idealized barotropic model of Charney and DeVore (1979), which we discussed in Sec. 2.2.

More complex models—both barotropic (i.e., single-layer) and baroclinic (i.e., multilayer), with more spatial degrees of freedom than the Charney and DeVore (1979) model—exhibit multiple flow patterns, some of which are similar to the blocked and zonal ones found in Fig. 1 above, even for fairly realistic values of the forcing. The crucial difference is that the equilibria found in the more complex models are no longer stable, and the system oscillates around the blocked solution or fluctuates between the zonal and blocked solutions in an irregular, chaotic way (Legras and Ghil, 1985; Ghil and Childress, 1987, ch. 6).

The Legras and Ghil (1985) model, for instance, has 25 spherical harmonics and its bifurcation diagram also appears as Fig. 8 in Ghil and Robertson (2002). In this diagram, the branch of blocked equilibria is destabilized by an oscillatory instability as the intensity of the forcing jet increases. The transition from a stable stationary solution — called a fixed point in dynamical systems theory — to a stable periodic solution, called a limit cycle in this theory, is termed a Hopf bifurcation. The limit cycle that arises from this bifurcation increases in amplitude as the forcing jet becomes stronger, and it has a period of roughly 40 days. This limit cycle loses its stability in turn as forcing is increased further and the flow becomes chaotic, but the 40-day periodicity survives in the power spectrum of the chaotic flow.

Jin and Ghil (1990) showed that, when a sufficiently realistic meridional structure of the solutions' zonal jet is allowed, the back-to-back saddle-node bifurcations of Fig. 1a are indeed replaced by a Hopf bifurcation

and thus transition to finite-amplitude periodic solutions can occur. Eigenanalyses of the unstable equilibria in a barotropic model with higher horizontal resolution, as well as its time-dependent solutions, indicate oscillatory instabilities with intraseasonal (35–50 days) and biweekly (10–15 days) time scales (Strong et al., 1993). Floquet analysis of this model's limit cycles (Strong et al., 1995) confirms that the 40-day oscillations that arise in it by oscillatory topographic instability are stronger in winter than in summer, like the observed NH oscillations (Ghil and Mo, 1991; Knutson and Weickmann, 1987).

To test the theory of NH extratropical oscillations developed in simpler models, Marcus et al. (1994, 1996) studied a 3-year perpetual-January simulation that had been performed with a version of the UCLA GCM in which no self-sustained MJO was apparent in the tropics. A robust 40-day oscillation in AAM is found to arise in the model's NH extratropics when standard topography is present. Three shorter runs with no topography produced no intraseasonal oscillation; this result is consistent with a topographic origin for the NH extratropical oscillation in the standard model. The spatial structure of the circulation anomalies associated with the model's extratropical oscillation is shown in an 8-minute video, `https://AAM_the_Video`, as displayed in several model-simulated fields, namely 500-hPa geopotential heights, 250-hPa streamfunction, and surface pressure torques.

The oscillation is dominated by a standing wavenumber-2 pattern, which undergoes a predominantly barotropic, tilted-trough vacillation. High values of AAM are associated with low 500-hPa heights over the northeast Pacific and the North Atlantic oceans, and vice versa. These flow patterns resemble the configurations seen in the Charney and DeVore (1979) simple model (see Fig. 1b here). The NE-SW–tilting and NW-SE–tilting phases in the video's 500-hPa fields are strongly reminiscent of the extremes and intermediate phases of the 40-day oscillation that arises by Hopf bifurcation from the blocked equilibrium in the Legras and Ghil (1985) model; see discussion of Ghil et al. (2003, Fig. 3).

4. Low-order data-driven modeling, dynamical analysis, and prediction

Linear and nonlinear LOMs and the role of memory effects. Empirical model reduction (EMR) & EMR-based prediction. Partial observations and stochastic closure in LOMs. Slow changes in the forcing and random effects: non-autonomous and random dynamical systems.

4.1. Background and methodological LOM developments

State-of-the-art, highly resolved GCMs, while able to simulate detailed interactions within the climate system over a wide range of scales, generate detailed 4-D climate variability that is visually as complex as currently available observational datasets, and is hence no less challenging to interpret. Dynamical analysis of climatic phenomena typically involves a set of multiple GCM simulations that are designed to isolate physical processes governing the simulated, and by inference, observed climate variability. These simulations are, however, computationally expensive, and their interpretation is hindered by the presence of model biases due to incomplete or imperfect parameterizations of the unresolved physical processes.

Moreover, GCMs represent a broad range of time and space scales and use a state vector that has many millions of scalar variables. While detailed weather prediction out to a few days does require such high numerical resolution, considerable work, both theoretical (Ghil and Childress, 1987, Sec. 6.5) and data-based (Toth, 1995), has shown that important aspects of observed atmospheric LFV can be represented and predicted with a substantially smaller number of degrees of freedom, as encapsulated by LOMs.

This statement extends beyond the issues of simulating and understanding LFV: it clearly includes prediction as well, and it is also consistent with the fact that climate concerns statistical time and space aggregates of weather. In fact, while there has been a recent surge of interest in S2S prediction through coordinated international modeling activity, most of this activity involves GCM-based ensemble prediction systems. Empirical, data-driven prediction, though, has a long history in forecasting the El Niño–Southern Oscillation (ENSO) and the best LOMs (e.g., Kondrashov et al., 2005) were still outperforming — no longer than six years ago — most GCM-based ENSO forecasts, even for lead times beyond the S2S range (Barnston et al., 2012). Unfortunately, since the Barnston et al. (2012) review paper, the plume of real-time Niño-3.4 predictions — which includes those of stochastic-dynamic models, as well as

of GCMs — that is continuously monitored at the International Research Institute for climate and society (IRI) no longer allows one to isolate the skill of individual LOMs or GCMs. Still, inspection of the existing documentation at https://iri.columbia.edu/our-expertise/climate/forecasts/enso/2017-October-quick-look/?enso_tab=enso-sst_table does indicate that — over the last seven boreal winters, 2012-13 to 2017-18 — ENSO prediction has remained a tough problem for both GCMs and simpler models. Hence, the contribution of the latter to real-time S2S forecasting can still be quite useful, in and of itself, as well as in stimulating improvements in GCM predictions.

A theoretical approach to LOM development relies on time scale separation in the full governing equations to derive a reduced set of differential equations for the LFV and to parameterize the fast, unresolved variability — such as atmospheric convection on synoptic and mesoscales — by stochastic forcing (e.g., Epstein, 1969; Fleming, 1971; Majda et al., 1999). An alternative approach to climate diagnosis and prediction is based on empirical modeling of the LFV, as observed in selected fields, under the assumption that it can be described as a spatio-temporal, nonlinear and stochastic process. This statistical data-driven approach does not require knowledge of the governing equations: even though it lacks the immediate dynamical interpretability of climate models that are derived from first principles, it does allow one to reproduce detailed aspects of the observed statistics by inverse modeling techniques, albeit in the subset of fields being simulated by the LOM. The available datasets — whether given by direct observations, reanalyses or GCM simulations — are used to estimate both the model's low-order, deterministic part and its driving noise.

Development of data-driven LOMs can thus be cast as a closure problem: These models can simulate and predict LFV provided they are able to properly account for (a) linear and nonlinear interactions between the resolved components, i.e., the high-variance LFV modes; and (b) the interactions between the resolved components and the huge number of unresolved ones that represent the unobserved small-scale processes and are not explicitly included in the LOM. The key steps are thus estimating interactions between the macroscopic variables, identifying the hidden variables, and modeling the cross-interactions between the macroscopic and hidden variables.

Linear inverse models (LIMs) and Principal Oscillation Pattern (POP) analysis (Penland, 1989; Penland and Ghil, 1993; Penland, 1996; Penland and Sardeshmukh, 1995) assume a linear dynamical model for the macroscopic variables, while their interactions with the small-scale, hidden processes are approximated by spatially correlated white noise. The Empirical Model Reduction (EMR) approach (Kravtsov et al., 2005, 2009; Kondrashov et al., 2013) generalizes LIMs by allowing (i) quadratic interactions among macroscopic variables; (ii) time-delayed dynamical effects via memory terms; and (iii) a richer temporal structure of the noise. The memory effects that may appear in both the stochastic forcing and the dynamical operator are conveyed by hidden variables arranged into a stacked system of levels. Each additional level includes a new hidden variable, which is less auto-correlated than the one included on the previous level, until the last-level variable can be approximated by spatially correlated white noise.

Chen et al. (2016) conducted a comprehensive suite of EMR experiments using a 4000-yr–long preindustrial control simulation dataset from the CM2.1 coupled model of NOAA's Geophysical Fluid Dynamics Laboratory (GFDL), with the goal of better understanding ENSO diversity, nonlinearity, seasonality and the effects of memory in the simulation and prediction of the Tropical Pacific's SST anomalies. The results show that multilevel nonlinear EMR models that account for SST history improve ENSO prediction skill dramatically.

The EMR model coefficients introduced on each level are estimated by multilevel regression techniques; see Kravtsov et al. (2009) for a comprehensive review of the EMR methodology. Strounine et al. (2010) have systematically compared various model reduction methods, as applied to wintertime geopotential height anomalies, and have demonstrated that, in the absence of clear scale separation, EMR methodology's success is rooted in its multilayer structure that accounts for the memory effects needed to achieve optimal closure (Kravtsov et al., 2005).

Newman et al. (2003) showed that, at the beginning of the past decade, the forecast skill of a LIM model of NH extratropical, weekly averaged circulation is comparable to that of NCEP's medium-range forecast (MRF) model at week 2 (days 8–14) and week 3 (days 15–21). Zhang et al. (2013) and Vitart (2017) have documented the progress in MJO simulation and prediction by GCMs since then. Thus, the best GCM predictions have achieved a bivariate correlation skill near 0.6 at four weeks, as measured between the two

observed and forecast Real-Time Multivariate MJO Indices known as RMM1 and RMM2.

At the same time, LOMs have also progressed beyond LIMs, as outlined above. Kondrashov et al. (2013) have improved upon the EMR-based predictions used in real-time ENSO forecasting (Kondrashov et al., 2005) by including in the forecast ensemble information on the "weather noise" that prevailed at particular phases of the MJO cycle, via the *past-noise forecasting (PNF)* methodology of Chekroun et al. (2011b). These authors have demonstrated that, in retrospective forecasting, PNF-enhanced EMR methodology yields bivariate-RMM correlation results that are quite comparable to those of the best GCMs (Kondrashov et al., 2013, Fig. 2).

More broadly speaking, EMR-based climate predictions have proven to be highly useful and competitive as statistical benchmarks against physics-based models for prediction on the S2S time scales associated with the MJO (Kondrashov et al., 2013), as well as with ENSO (Kondrashov et al., 2005).

The Multilayer Stochastic Model (MSM) framework introduced by Kondrashov et al. (2015) establishes, in a data-driven context, a clear connection between the EMR methodology and the Mori-Zwanzig (MZ) formalism of statistical physics. It is this sound physical basis that helps derive a closed system of stochastic-dynamic equations for a subset of the original system's variables (Kondrashov et al., 2015, Secs. 4 & 5). This closed system of equations includes Markovian and non-Markovian deterministic terms that are not necessarily quadratic, as well as stochastic noise terms (Chorin et al., 2002; Chorin and Hald, 2006).

The major methodological problem is that, in the highly nonlinear climate system, there is typically a continuum of scales, from the fastest and shortest to the slowest and longest. In this case, the MZ formalism allows one to treat the interactions between LFV and smaller scales as memory effects. These memory effects represent a significant deviation from the markovianity of the dynamical models that are most often used in modeling atmospheric, oceanic and climate phenomena and processes. Markovianity means dependence on the initial state alone, as opposed to states that preceded it. Thus, ordinary and partial differential equations, as well as the Markov chains mentioned in Sec. 2 herein, are markovian: delay-differential and other functional differential equation (Hale and Verduyn Lunel, 1993) are not. Bhattacharya et al. (1982) introduced the latter into the climate sciences and they have been used since extensively in ENSO modeling, with memory terms that account for travel times of Kelvin and Rossby waves across the Tropical Pacific; see also (Ghil et al., 2015, and references therein).

The non-Markovian terms become particularly important in the absence of scale separation, whereas Stinis (2006) showed that, for relatively large scale separation, the results of the MZ methodology are similar to those of the model reduction formalism of Majda et al. (1999). The MSM framework thus improves upon EMR by its greater generality of the deterministic terms, as well as by the proper understanding of the memory effects. The improvements in simulation and prediction achieved by nonlinear (EMR and MSM) vs. linear (LIM and POP) data-driven models (e.g., Barnston et al., 2012) seem to further buttress the credibility of the highly nonlinear Devil's staircase scenario for ENSO (Jin et al., 1994; Tziperman et al., 1994) vs. stable noise-forced dynamics (Neelin et al., 1998).

Kondrashov and Berloff (2015) have shown that a change of basis by M-SSA can help in applying the MSM methodology to capture the LFV in multiscale oceanic turbulence, because M-SSA utilizes time-lagged information and therefore implicitly conveys the memory effects. Data-adaptive harmonic decomposition (DAHD: Chekroun and Kondrashov, 2017) further advances the dynamic interpretation of nonlinear data-driven models. DAHD provides, for a broad class of time-evolving datasets, reduction coordinates that can be efficiently modeled by systems of paired stochastic differential equations (SDEs), while using a fixed set of predictor functions. The methodology has proven itself already in the modeling, simulation and prediction of the Arctic's sea ice extent and concentration field (Kondrashov et al., 2017a,b), but remains to be tested for other climatic time series.

In summary, the field of low-order, data-driven stochastic-dynamic models has undergone remarkable development in recent years. These models offer, therewith, new opportunities to further our understanding and prediction on S2S time scales. The following two subsections present examples of their successful application to mid-latitude LFV variability and to ENSO phenomena, respectively.

4.2. Dynamical diagnostics and empirical prediction on S2S scales

LOMs can be very useful for the dynamical interpretation of atmospheric oscillations and multiple regimes. Such models not only help compact the dataset's information content but can also provide insights into the dynamics and predictability of climatic LFV, via the analysis of the reduced model's mathematical structure. Thus, Kondrashov et al. (2006, 2011) constructed and analyzed a LOM of extratropical atmospheric LFV by applying EMR to the output of a long simulation of the QG3 model mentioned in Sec. 2.2. This model has a fairly realistic climatology and variability, and it has been used quite extensively to study NH mid-latitude flows (e.g., D'Andrea and Vautard, 2001; D'Andrea, 2002; Deloncle et al., 2007, and references therein).

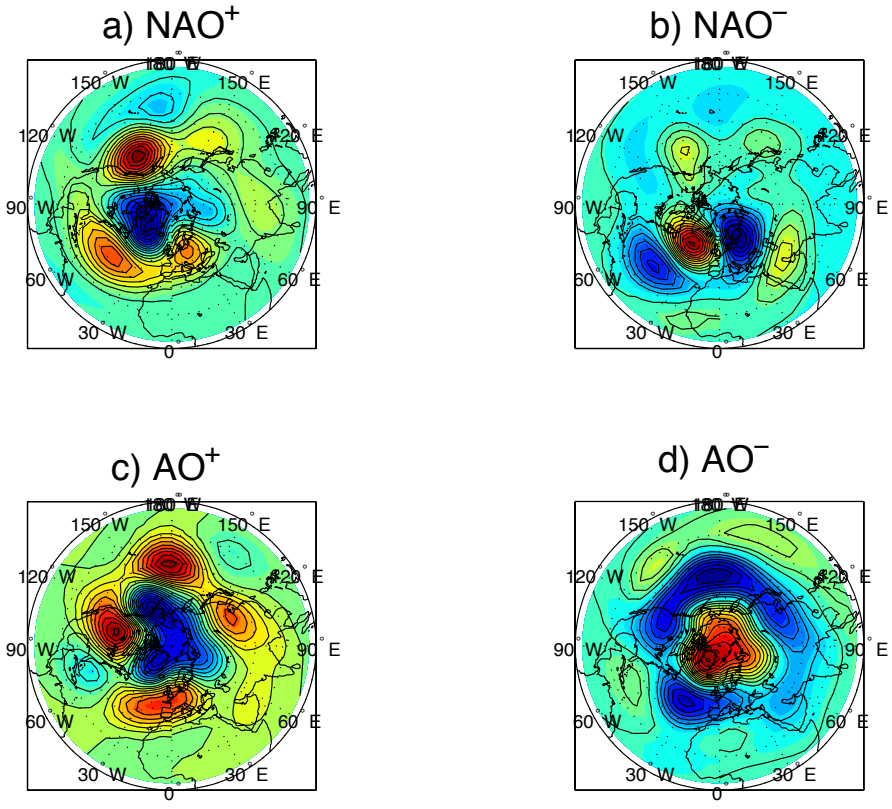

Figure 7: Gaussian mixture-model centroids, showing streamfunction anomaly maps at 500 hPa, for the QG3 model: (a) NAO^+; (b) NAO^-; (c) AO^+; and (d) AO^-. Positive contours are solid and land masses are shaded; twenty contour levels between maximum and minimum values are used, with the following intervals (in 10^6 $m^2\,s^{-1}$): (a) 1.1; (b) 0.8; (c) 0.8; and (d) 1.1. After Kondrashov et al. (2006). (©American Meteorological Society. Reproduced with permission.)

The full QG3 model's phase space has a dimension of $\mathcal{O}(10^4)$, while the derived EMR model has only 45 variables. The regimes of both the EMR model and the QG3 model were computed using a Gaussian mixture model by following Smyth et al. (1999, and references therein). The centroids of the four regimes for the full QG3 model are plotted in Fig. 7, and they correspond to opposite phases of the Arctic Oscillation (AO^+ and AO^-) and of the North Atlantic Oscillation (NAO^+ and NAO^-), in good agreement with the earlier results of Molteni and Corti (1998). The EMR model captures very well the non-Gaussian features of the full QG3 model's probability density function (PDF) and shares with the latter its four anomalously

persistent flow patterns, as well as the Markov chain of transitions between these regimes (not shown).

The spatial correlations between the anomaly patterns in Fig. 7 and those of the EMR model (not shown) all exceed 0.9. This good match between the regime centroids in the two models, full and reduced, as well as between the corresponding Markov chains, emphasizes the intrinsic dynamical nature of both the NAO and the AO, and strongly suggests that the NAO is not merely a regionalization of the AO, at least not in the fairly realistic QG3 model.

The four regimes that are best supported by synoptic experience, as well as by the statistical analysis of the upper-air data for the past half-century, are the zonal and blocked phases of westerly flow in the Atlantic–Eurasian and Pacific–North-American sector, respectively (Cheng and Wallace, 1993; Smyth et al., 1999; Ghil and Robertson, 2002). The AO, also called the NH annular mode (Wallace, 2000), seems to be only statistically annular: it representa a redistribution of mass between the poles and subtropics, but actual "sloshing" events are sectorial, by-and-large. Hence the correlation between the subtropical highs over the North Atlantic and the North Pacific in observational and reanalysis data is quite low at sub-monthly time scales (e.g., Kimoto and Ghil, 1993b).

Both the AO and NAO indices are, however, dominated by Arctic sea-level pressure variations, and hence the NAO and AO are highly correlated in observations. Moreover, both the QG3 model (Kondrashov et al., 2006) and the no-MJO version of the UCLA GCM (Marcus et al., 1994, 1996) seem to possess some form of a 40-day sloshing mode that originates in mid-latitudes. Seeing the hemispheric AO^+ and AO^- patterns of Figs. 7(c,d) replace the PNA-sector patterns of Ghil and Robertson (2002, and references therein) is thus not too surprising: the hemispheric $AO^{\pm}$ centroids overlap largely in the Atlantic–Eurasian sector with $NAO^{\pm}$, respectively, from which they differ mainly by much stronger centers of action in the PNA sector.

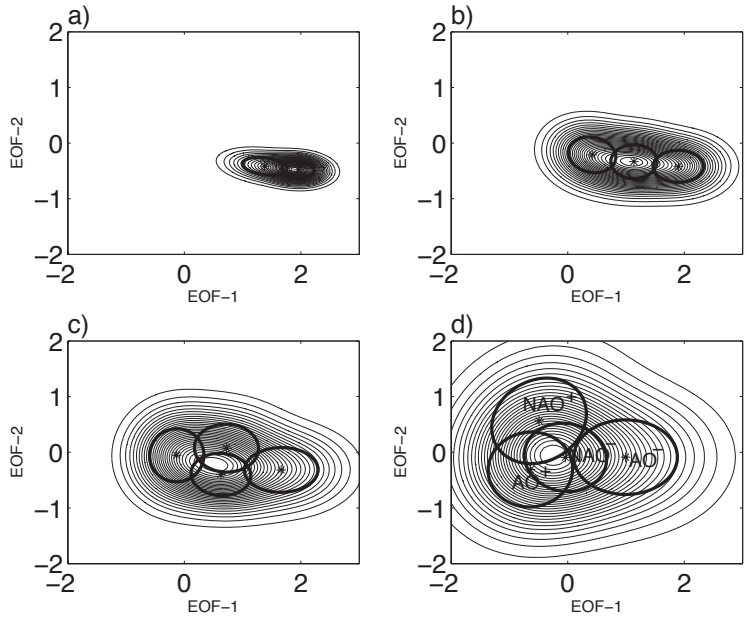

Figure 8: Mixture-model clusters for EMR model simulations of the full QG3 atmospheric model. The four panels differ by the amplitude of the EMR's stochastic forcing, which is multiplied by a factor ϵ: a) $\epsilon = 0.2$; b) $\epsilon = 0.4$; c) $\epsilon = 0.6$; d) $\epsilon = 1$ (optimal case). Note that the number of the clusters and their separation in phase space increase with ϵ. The four regimes are only labeled in panel (d). After Kondrashov et al. (2006) (©American Meteorological Society. Reproduced with permission.)

In addition, M-SSA identifies intraseasonal oscillations with a period of 35–37 days and of 20 days in the data generated by both the full QG3 model and its EMR version. These oscillatory modes are similar to those seen in the observations, as plotted in Fig. 3 here, and in previous studies (e.g., Ghil and Robertson, 2000, 2002, and references therein). The former one is clearly these models' version of the extratropical,

40-day mode found by Legras and Ghil (1985), while the QG3 model is expected to lack the MJO-related 50-day mode seen in Fig. 3. Lott et al. (2001, 2004a,b) have shown that observational NH data confirm the importance of mountain torques in an extratropical oscillation that has a shorter periodicity than the MJO. Mountain torque anomalies were also found to anticipate the phases of the AAM oscillation, as well as the onsets and breaks of certain flow regimes.

The QG3 model's LFV features can be interpreted via dynamical analysis of the reduced model. In particular, the AO^- regime arises from the unique steady state of the EMR model's three-level deterministic operator, at the larger positive values of PC-1, while the PDF ridge that is present in the QG3 model, cf. Kondrashov et al. (2006, Fig. 6), coincides with the location of a plateau of quasi-stationary states of the reduced model, cf. Figs. 8(b–d) here. The increase of the extent of the PDF plateau in both the full and the reduced model — first along the EOF-1 direction and then, at lower negative values of PC-1, along the EOF-2 direction — appears to be due to preferential instabilities in the subspace of the QG3 model's leading modes. These instabilities are to be equilibrated by the full model's transient feedbacks that are captured in the EMR by the noise and memory effects.

Changes in the number and amplitude of the PDF's modes were also observed by Molteni and Corti (1998) when varying the potential vorticity forcing in the QG3 model to represent a subtropical Rossby wave source appropriate for cold ENSO events. The changes plotted in Fig. 8 here can be interpreted as changes that might arise in a GCM subject either to stochastic parametrizations with varying noise intensities (e.g., Palmer and Williams, 2009, and references therein) or to fluctuating changes in external forcing. The rather surprising succes of EMRs, in their various guises, at simulating and predicting S2S variability may be largely attributed to the presence and proper intensity of the noise processes they include.

The dominant intraseasonal oscillation in both the QG3 and the optimal EMR model has a period of about 35–37 days and it is associated with the least-damped eigenmode of the latter, when linearized about its climatological state. While there is no clear scale separation in the QG3 simulations, it is the interactions between the model's largest-scale modes — whose variance is concentrated in the subspace of its four leading EOFs — and the intermediate scales, captured by EOFs 5–15, that appear to be responsible for the slow-down of the intraseasonal oscillation's trajectory in the full QG3 model, as well as in the optimal EMR model. This slow-down is associated with the emergence of the AO^+ and NAO^- regimes.

The EMR model's stochastic forcing represents the unresolved smaller-scale processes in the QG3 model. The effect of this forcing on the full dynamics is revealed by a bifurcation analysis with respect to the noise's amplitude ϵ. In particular, Fig. 8 shows that, as ϵ increases from zero to its optimal value, the model trajectory is initially confined to a small region near the EMR model's unique steady state (panel (a)) and that it gradually fills up the quasi-stationary ridge along the EOF-1 axis (panels (b)–(d)). When ϵ becomes large enough, the intraseasonal oscillatory mode is excited, resulting in the model's PDF expanding in the EOF-2 and EOF-3 directions, while additional quasi-stationary states appear. The sequence of panels in Fig. 8 can be taken to imply that the stochastic forcing needs to be sufficiently strong in order to obtain realistic LFV regimes. The role of stochastic processes in nonlinear dynamics will be discussed more fully at the end of this chapter, in Sec. 5.

Kondrashov et al. (2011) have also analyzed this EMR model's nonlinear dynamical operator and shown that it gives rise to "swirls" in the time-mean tendencies of the model's state-averaged trajectories, when projected onto a low-dimensional subspace. These swirls are dominated by the deterministic interactions between the large-scale modes. More recently, Tantet et al. (2015) have associated similar swirl patterns with persistent weather regimes in the output of a barotropic atmospheric model with an intermediate resolution of 231 spherical modes. These authors applied transfer operator methods (Chekroun et al., 2014, and references therein) to develop early warning indicators for regime transitions, in particular from zonal to blocked flows, as mentioned in Sec. 2.2.

The idea of considering preferred directions of instability of a regime's centroid goes back to the "ghost equilibria" of Legras and Ghil (1985). In particular, Deloncle et al. (2007) and Kondrashov et al. (2007) have applied the random forests algorithm (Breiman, 2001) to learn the predictors connected to these preferred directions in a low-dimensional space. This statistical approach worked rather well in medium-to-long-range prediction of regime breaks, in both the QG3 model (Deloncle et al., 2007) and NH atmospheric observational data (Kondrashov et al., 2007). The results of Tantet et al. (2015) provide further dynamical understanding

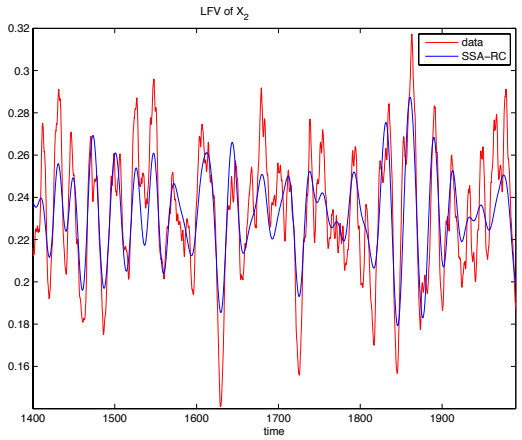

Figure 9: Time series of the component x_2 (red curve) and its LFV mode obtained by SSA reconstruction (blue curve). The latter has a dominant period of 25 nondimensional units, and it captures 36% of the total variance.

for why that appears to be the case. In the context of S2S prediction, the dynamically motivated predictors might turn out to correspond to preferred instability directions of either fixed points that "anchor" multiple regimes, such as El Niño and La Niña (Dijkstra, 2005, Ch. 7, and references therein), or to similar instabilities of limit cycles that are associated with oscillatory modes, such as the MJO or the extratropical, 40-day mode discussed in Sec. 3.1 and the present one. Instability of limit cycles in atmospheric LFV was studied, for instance, by Strong et al. (1995), and is mentioned here in Sec. 3.2.

4.3. LFV and multilayer stochastic closure: A simple illustration

In this subsection, we provide an illustrative example that will help understand the reasons for the effectiveness of MSM modeling, and hence of EMR models, in simulating and potentially predicting extratropical S2S variability. This example illustrates intraseasonal ENSO prediction.

Consider the following nonlinear, periodically and stochastically forced two-variable (x_1, x_2) model from Chekroun et al. (2011b, Supplementary Information):

$$\begin{cases} \mathrm{d}x_1 = \{(r + \sigma \mathrm{d}W_t)x_1(\alpha + x_1)(1 - x_1) - cx_1x_2 + a\sin(2\pi f_0 t)\}\mathrm{d}t, \\ \mathrm{d}x_2 = \{-m\alpha x_2 + (c - m)x_1x_2\}\mathrm{d}t. \end{cases} \tag{1}$$

Here the variable x_1 is subject to deterministic, additive forcing $a\sin(2\pi f_0 t)$, while the stochastic term $\sigma \mathrm{d}W_t$ represents a random perturbation of the parameter r by white noise, and we assume that only the variable x_2 is observed. The default values of the model parameters are $\sigma = 0.3$, $m = r = 1$, $c = 1.5$ and $\alpha = 0.3$. The model is integrated from time $t = 0$ to $t = T_\mathrm{f} = 2000$ (in dimensionless units), with the initial state $(x_1(0), x_2(0)) = (0.5, 0.5)$, by using a classical stochastic Euler-Maruyama scheme with step size $\Delta t = 0.1$. When both periodic forcing and noise are absent, the model has only one globally stable equilibrium.

When turning on the periodic forcing with amplitude $a = 0.05$ and frequency $f_0 = 0.25$, the system exhibits only one periodic orbit of period 4, which is globally stable. In the presence of noise, with $\sigma = 0.3$, an LFV mode with a period equal to approximately 25 units — i.e., a frequency of $f = 0.04 \neq f_0$ — becomes dominant, as seen in Fig. 9. This mode (blue in the figure) is captured by SSA reconstruction, and it can be attributed to a damped non-normal mode that is sustained by the noise (Chekroun et al., 2011b). In the present ENSO-related illustration, the periodic forcing $T_0 = 1/f_0 = 4$ corresponds to the seasonal cycle, while the intrinsic periodicity of $T \simeq 25$ is associated with ENSO's low-frequency mode of roughly 6 years.

By applying EMR solely to a time series of the observed variable x_2, cf. Kravtsov et al. (2005), a univariate two-level EMR model is obtained for x_2 alone. This scalar model includes a cubic polynomial, as well as

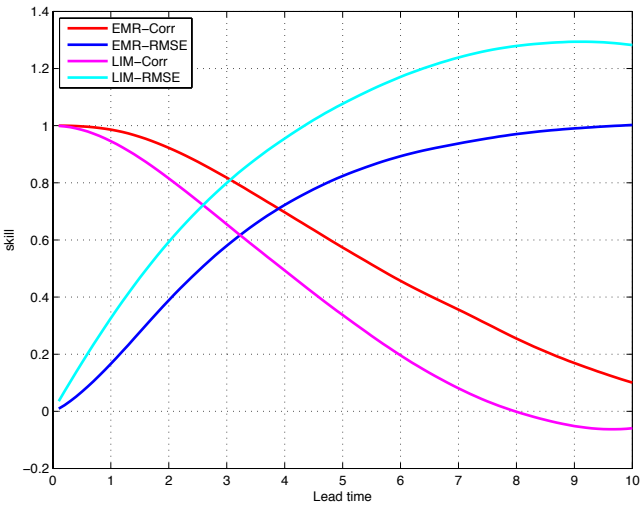

Figure 10: Prediction skill for the optimal EMR model obtained solely from the $x_2(t)$ time series. The best cubic two-level EMR model clearly outperforms LIM both in terms of anomaly correlations (red curve vs. magenta) and root-mean-square (RMS) errors (blue vs. cyan).

multiplicative interaction with the periodic forcing, on its main level (not shown). Note that this parametric form is entirely different from the correct form of the right-hand side of the x_2-equation in Eq. (1), as it does not explicitly include interactions with the periodically and stochastically forced unobserved variable x_1. These interactions are parameterized by the memory effects conveyed in the two-level EMR model.

Prediction skill is plotted in Fig. 10 in terms of both root-mean-square errors (RMSE) and anomaly correlations (Corr). The figure shows that the out-of-sample prediction skill of the ensemble mean for the estimated EMR model is significantly better than that of a linear single-level LIM model, with the EMR's maintaining useful prediction skill, i.e. Corr≥ 0.5, up to a lead time of roughly 6 time units, which represents roughly a quarter of a period of the LFV mode.

This example illustrates the benefits for prediction of including nonlinear and memory terms in empirical stochastic models, as demonstrated by comparing the performance of UCLA's EMR model in real-time ENSO forecasting with other statistical forecasts; see Barnston et al. (2012).

5. Concluding remarks

Considerable progress has been made in the 15 years since the review article of Ghil and Robertson (2002) in low-order predictive modeling of what was called at that time extended or long-range forecasting and is now more specifically referred to as S2S prediction. Four of the approaches that were considered in this modeling are summarized in Fig. 11.

One approach to persistent anomalies in mid-latitude atmospheric flows on 10–100-day time scales is to consider them simply as due to slowing down of Rossby waves or to their linear interference (Lindzen et al., 1982; Lindzen, 1986). This approach is illustrated in the sketch labeled (c) within the figure: zonal flow Z and blocked flow B are simply slow phases of an harmonic oscillation, like the neighborhood of $t = \pi/2$ or $t = 3\pi/2$ for a sine wave $\sin(t)$; or else they are due to an interference like that occurring for a sum $A\sin(t) + B\sin(3t)$ near $t = (2k+1)\pi/2$. A more thorough, quasi-linear version of this approach is to study long-lived resonant wave triads between a topographic Rossby wave and two free Rossby waves (Egger, 1978; Trevisan and Buzzi, 1980; Ghil and Childress, 1987, Section 6.2). Neither version of this approach, though, explains the anomalies' organizing into distinct flow regimes.

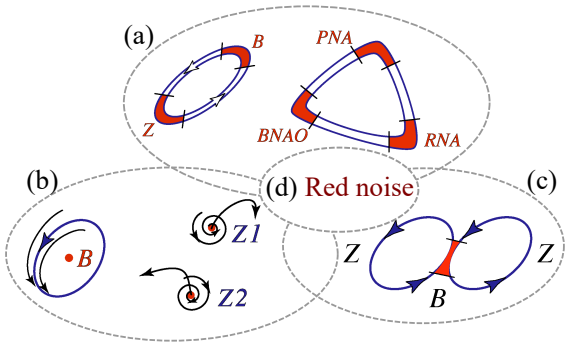

Figure 11: Schematic overview of atmospheric LFV mechanisms.

Rossby et al. (1939) initiated a different, genuinely nonlinear approach by raising the possibility of multiple equilibria as an explanation of preferred atmospheric flow patterns. These authors drew an analogy between such equilibria and hydraulic jumps, and formulated simple models in which similar transitions between faster and slower atmospheric flows could occur. This multiple-equilibria approach was then pursued quite agressively in the 1980s (Charney and DeVore, 1979; Charney et al., 1981; Legras and Ghil, 1985; Ghil and Childress, 1987, Sections 6.3–6.6) and it is illustrated in Fig. 11 by the sketch labeled (a): one version of the sketch illustrates models that concentrated on the B–Z dichotomy (Charney and DeVore, 1979; Charney et al., 1981; Benzi et al., 1986), the other on models (e.g., Legras and Ghil, 1985) that allowed for the presence of additional clusters, like those found by Kimoto and Ghil (1993a) or Smyth et al. (1999), viz. opposite phases of the NAO and PNA anomalies (PNA, RNA and $BNAO \simeq NAO^-$ in sketch (a) of Fig. 11). The LFV dynamics in this approach is given by the preferred transition paths between the two or more regimes; see again Table 1 in Sec. 2.1 and references therein.

A third approach is associated with the idea of oscillatory instabilities of one or more of the multiple fixed points that can play the role of regime centroids. Thus, Legras and Ghil (1985) found a 40-day oscillation arising by Hopf bifurcation off their blocked regime B, as illustrated in sketch (b) of the figure. An ambiguity arises, though, between this point of view and a complementary possibility, namely that the regimes are just slow phases of such an oscillation, caused itself by the interaction of the mid-latitude jet with topography, cf. Sec. 3.2. Thus, Kimoto and Ghil (1993b) found, in their observational data, closed paths within a Markov chain whose states resemble well-known phases of an intraseasonal oscillation. Such a possibility was confirmed in the QG3 model by Kondrashov et al. (2004). Furthermore, multiple regimes and intraseasonal oscillations can coexist in a two-layer model on the sphere within the scenario of "chaotic itinerancy" (Itoh and Kimoto, 1996, 1997).

Finally, sketch (d) in the figure refers to the role of stochastic processes in S2S variability and prediction, whether it be noise that is white in time — as in Hasselmann (1976) or in LIMs (Penland, 1989, 1996; Penland and Ghil, 1993; Penland and Sardeshmukh, 1995) — or red in time, as in EMRs and MSMs (Kravtsov et al., 2005, 2009; Kondrashov et al., 2006, 2013, 2015) or even non-Gaussian (Sardeshmukh and Penland, 2015). Stochastic processes may enter into models situated on various rungs of the modeling hierarchy, from the simplest conceptual models to high-resolution GCMs. In the latter, they may enter via stochastic parametrizations of subgrid-scale processes (e.g., Palmer and Williams, 2009, and references therein), while in the former they may enter via stochastic forcing, whether additive or multiplicative, Gaussian or not (e.g., Kondrashov et al., 2015, and references therein).

Figure 11 simply summarizes some of the key dynamical mechanisms of mid-latitude S2S variability, as discussed in this chapter, without providing a definitive answer to which approach to low-order modeling and prediction is or will be most productive in the near future. Such an answer is likely to be long in coming, if ever. On the more practical aspects of S2S prediction, though, it is clear that the ideas presented herein — on the role of LOMs vs. more detailed and highly resolved models, and on extratropical sources of variability and hence of predictability — are certain to be of use. The most promising LOMs appear to be those that do include nonlinear dynamics, memory effects, and colored noise. EMRs and MSMs that do

so have proven quite competitive in ENSO forecasting, according to Barnston et al. (2012), and are likely to provide important prediction benchmarks for S2S forecasting, as well as important tools for a more complete understanding of the dynamics of extratropical S2S variability and teleconnections.

We conclude with a few comments about the role of climate change in the S2S variability and predictability problem. As mentioned in Sec. 1, the difficulty of the S2S problem is largely due to its being mid-way between the short-term weather problem and the long-term climate problem (Von Neumann, 1955). A mathematically self-consistent way out of this difficulty is provided by the theory of non-autonomous and random dynamical systems, as introduced recently into the climate sciences (e.g., Ghil et al., 2008; Chekroun et al., 2011a; Drótos et al., 2015; Ghil, 2017, and references therein). This theory — as opposed to the classical theory of autonomous dynamical systems, in which coefficients and forcing do not depend on time — allows one to include very fast forcing, by stochastic processes, as well as much slower forcing. Examples of the latter include not only changes in radiative forcing due to anthropogenic changes in aerosol and greenhouse gas concentrations, but also forcing by ocean–atmosphere (e,g., Ghil, 2001, 2017, and references therein) or stratosphere–troposphere interactions (e,g., Holton et al., 1995, and references therein). There is no room here to either provide a more detailed account of the appropriate concepts and methods or to actually apply it to NH LFV. Fairly readable accounts for the climate scientist do exist, though (Ghil, 2014; Moron et al., 2015; Chang et al., 2015, Ch. 2), and might encourage the interested reader to use them in the S2S context.

Acknowledgments. It is a pleasure to acknowledge detailed and constructive comments by Fréderic Vitart and an anonymous reviewer. This work was partially supported by U.S. Office of Naval Research under MURI grants N00014-12-1-0911 and N00014-16-1-2073.

References

Alessio, S.M., 2016. Digital Signal Processing and Spectral Analysis for Scientists: Concepts and Applications. Springer. URL: http://www.springer.com/us/book/9783319254661.

Barnston, A.G., Tippett, M.K., Heureux, M.L., Li, S., DeWitt, D.G., 2012. Skill of real-time seasonal ENSO model predictions during 2002–2011 — is our capability improving? Bulletin of the American Meteorological Society 93, 631–651. doi:10.1175/BAMS-D-11-00111.1.

Benzi, R., Malguzzi, P., Speranza, A., Sutera, A., 1986. The statistical properties of general atmospheric circulation: observational evidence and a minimal theory of bimodality. Quarterly Journal of the Royal Meteorological Society 112, 661–674. doi:10.1256/smsqj.47305.

Bhattacharya, K., Ghil, M., Vulis, I.L., 1982. Internal variability of an energy-balance model with delayed albedo effects. Journal of the Atmospheric Sciences 39, 1747–1773.

Bjerknes, V., 1904. Das Problem der Wettervorhersage, betrachtet vom Standpunkte der Mechanik und der Physik. Meteorologische Zeitschrift 21, 1–7.

Branstator, G., 1987. A striking example of the atmosphere's leading traveling pattern. Journal of the Atmospheric Sciences 44, 2310–2323. doi:10.1175/1520-0469(1987)044<2310:aseota>2.0.co;2.

Breiman, L., 2001. Random forests. Machine Learning 45, 5–32.

Brunet, G., Methven, J., 2018. Identifying wave processes associated with predictability across time scales: An empirical normal mode approach, in: Robertson, A.W., Vitart, F. (Eds.), The Gap Between Weather and Climate Forecasting: Sub-Seasonal to Seasonal Prediction. Elsevier. chapter 4, p. 40 pp.

Cassou, C., 2008. Intraseasonal interaction between the Madden–Julian Oscillation and the North Atlantic Oscillation. Nature 455, 523–527. doi:10.1038/nature07286.

Chang, C.P., Ghil, M., Latif, M., Wallace, J.M. (Eds.), 2015. Climate Change: Multidecadal and Beyond. World Scientific.

Charney, J.G., DeVore, J.G., 1979. Multiple flow equilibria in the atmosphere and blocking. Journal of the Atmospheric Sciences 36, 1205–1216. doi:10.1175/1520-0469(1979)036<1205:mfeita>2.0.co;2.

Charney, J.G., Shukla, J., Mo, K.C., 1981. Comparison of a barotropic blocking theory with observation. Journal of the Atmospheric Sciences 38, 762–779. doi:10.1175/1520-0469(1981)038<0762:coabbt>2.0.co;2.

Charney, J.G., Straus, D.M., 1980. Form-drag instability, multiple equilibria and propagating planetary waves in baroclinic, orographically forced, planetary wave systems. Journal of the Atmospheric Sciences 37, 1157–1176. doi:10.1175/1520-0469(1980)037<1157:fdimea>2.0.co;2.

Chekroun, M., Neelin, J., Kondrashov, D., McWilliams, J., Ghil, M., 2014. Rough parameter dependence in climate models: The role of Ruelle-Pollicott resonances. Proceedings of the National Academy of Sciences 111, 1684–1690. doi:10.1073/pnas.1321816111. doi:10.1073/pnas.1321816111.

Chekroun, M., Simonnet, E., Ghil, M., 2011a. Stochastic climate dynamics: Random attractors and time-dependent invariant measures. Physica D 240, 1685–1700. doi:10.1016/j.physd.2011.06.005.

Chekroun, M.D., Kondrashov, D., 2017. Data-adaptive harmonic spectra and multilayer Stuart-Landau models. Chaos 27, 093110. doi:10.1063/1.4989400.

Chekroun, M.D., Kondrashov, D., Ghil, M., 2011b. Predicting stochastic systems by noise sampling, and application to the El Niño-Southern Oscillation. Proceedings of the National Academy of Sciences 108, 11766–11771. doi:10.1073/pnas.1015753108.

Chen, C., Cane, M.A., Henderson, N., Lee, D.E., Chapman, D., Kondrashov, D., Chekroun, M.D., 2016. Diversity, nonlinearity, seasonality, and memory effect in ENSO simulation and prediction using empirical model reduction. Journal of Climate 29, 1809–1830. doi:10.1175/JCLI-D-15-0372.1.

Cheng, X., Wallace, J.M., 1993. Cluster analysis of the Northern Hemisphere wintertime 500-hPa height field: Spatial patterns. Journal of the Atmospheric Sciences 50, 2674–2696. doi:10.1175/1520-0469(1993)050<2674:caotnh>2.0.co;2.

Chorin, A.J., Hald, O.H., 2006. Stochastic Tools in Mathematics and Science. Number 147 in Surveys and Tutorials in the Applied Mathematical Sciences, Springer, New York.

Chorin, A.J., Hald, O.H., Kupferman, R., 2002. Optimal prediction with memory. Physica D 166, 239–257. doi:10.1016/s0167-2789(02)00446-3.

Christensen, H.M., Moroz, I.M., Palmer, T.N., 2014. Simulating weather regimes: impact of stochastic and perturbed parameter schemes in a simple atmospheric model. Climate Dynamics 44, 2195–2214. doi:10.1007/s00382-014-2239-9.

Corti, S., Molteni, F., Palmer, T.N., 1999. Signature of recent climate change in frequencies of natural atmospheric circulation regimes. Nature 398, 799–802. doi:10.1038/19745.

Crommelin, D.T., 2003. Regime transitions and heteroclinic connections in a barotropic atmosphere. Journal of the Atmospheric Sciences 60, 229–246. doi:10.1175/1520-0469(2003)060<0229:rtahci>2.0.co;2.

Crommelin, D.T., 2004. Observed nondiffusive dynamics in large-scale atmospheric flow. Journal of the Atmospheric Sciences 61, 2384–2396. doi:10.1175/1520-0469(2004)061<2384:ondila>2.0.co;2.

D'Andrea, F., 2002. Extratropical low-frequency variability as a low-dimensional problem. II: Stationarity and stability of large-scale equilibria. Quarterly Journal of the Royal Meteorological Society 128, 1059–1073. doi:10.1256/003590002320373201.

D'Andrea, F., Vautard, R., 2001. Extratropical low-frequency variability as a low-dimensional problem I: A simplified model. Quarterly Journal of the Royal Meteorological Society 127, 1357–1374. doi:10.1256/smsqj.57412.

Dawson, A., Palmer, T.N., 2014. Simulating weather regimes: impact of model resolution and stochastic parameterization. Climate Dynamics 44, 2177–2193. doi:10.1007/s00382-014-2238-x.

Dee, D.P., Uppala, S.M., Simmons, A.J., Berrisford, P., Poli, P., et al., S.K., 2011. The ERA-interim reanalysis: configuration

and performance of the data assimilation system. Quarterly Journal of the Royal Meteorological Society 137, 553–597. doi:10.1002/qj.828.
Deloncle, A., Berk, R., D'Andrea, F., Ghil, M., 2007. Weather regime prediction using statistical learning. Journal of the Atmospheric Sciences 64, 1619–1635. doi:10.1175/jas3918.1.
Deremble, B., Simonnet, E., Ghil, M., 2012. Multiple equilibria and oscillatory modes in a mid-latitude ocean-forced atmospheric model. Nonlinear Processes in Geophysics 19, 479–499. doi:10.5194/npg-19-479-2012.
Dickey, J.O., Ghil, M., Marcus, S.L., 1991. Extratropical aspects of the 40–50 day oscillation in length-of-day and atmospheric angular momentum. Journal of Geophysical Research: Atmospheres 96, 22643–22658. doi:10.1029/91jd02339.
Dijkstra, H.A., 2005. Nonlinear Physical Oceanography: A Dynamical Systems Approach to the Large Scale Ocean Circulation and El Niño. 2nd ed., Springer.
Dijkstra, H.A., 2013. Nonlinear Climate Dynamics. Cambridge University Press, Cambridge.
Dijkstra, H.A., Ghil, M., 2005. Low-frequency variability of the large-scale ocean circulation: A dynamical systems approach. Reviews of Geophysics 43, RG3002. doi:10.1029/2002RG000122.
Dole, R.M., Gordon, N.D., 1983. Persistent anomalies of the extratropical Northern Hemisphere wintertime circulation: Geographical distribution and regional persistence characteristics. Monthly Weather Review 111, 1567–1586. doi:10.1175/1520-0493(1983)111<1567:paoten>2.0.co;2.
Drótos, G., Bódai, T., Tél, T., 2015. Probabilistic concepts in a changing climate: A snapshot attractor picture. Journal of Climate 28, 3275–3288. doi:10.1175/jcli-d-14-00459.1.
Egger, J., 1978. Dynamics of blocking highs. Journal of the Atmospheric Sciences 35, 1788–1801. doi:10.1175/1520-0469(1978)035<1788:dobh>2.0.co;2.
Epstein, E.S., 1969. Stochastic dynamic prediction. Tellus A 21, 739–759.
Feliks, Y., Ghil, M., Robertson, A.W., 2010. Oscillatory climate modes in the Eastern Mediterranean and their synchronization with the North Atlantic Oscillation. Journal of Climate 23, 4060–4079. doi:10.1175/2010jcli3181.1.
Fleming, R.J., 1971. On stochastic dynamic prediction: I. The energetics of uncertainty and the question of closure. Monthly Weather Review 99, 851–872.
Ghil, M., 1987. Dynamics, statistics and predictability of planetary flow regimes, in: Nicolis, C., Nicolis, G. (Eds.), Irreversible Phenomena and Dynamical Systems Analysis in the Geosciences. D. Reidel, Dordrecht/Boston/Lancaster, pp. 241–283.
Ghil, M., 2001. Hilbert problems for the geosciences in the 21st century. Nonlinear Processes in Geophysics 8, 211–211. doi:10.5194/npg-8-211-2001.
Ghil, M., 2014. Climate variability: Nonlinear and random aspects, in: G. R. North, J.P., Zhang, F. (Eds.), Encyclopedia of Atmospheric Sciences. 2nd ed.. Elsevier. volume 2, pp. 38–46.
Ghil, M., 2017. The wind-driven ocean circulation: Applying dynamical systems theory to a climate problem. Discrete and Continuous Dynamical Systems. Series A 37, 189–228. doi:10.3934/dcds.2017008.
Ghil, M., Allen, M.R., Dettinger, M.D., Ide, K., Kondrashov, D., Mann, M.E., Robertson, A.W., Saunders, A., Tian, Y., Varadi, F., Yiou, P., 2002. Advanced spectral methods for climatic time series. Reviews of Geophysics 40, 1003. doi:10.1029/2000GR000010.1029.
Ghil, M., Chekroun, M., Simonnet, E., 2008. Climate dynamics and fluid mechanics: Natural variability and related uncertainties. Physica D 237, 2111–2126. doi:10.1016/j.physd.2008.03.036.
Ghil, M., Chekroun, M.D., Stepan, G., 2015. A collection on 'climate dynamics: multiple scales and memory effects', in: Ghil, M., Chekroun, M.D., Stepan, G. (Eds.), Proceedings of the Royal Society A. The Royal Society. volume 471, p. 20150097.
Ghil, M., Childress, S., 1987. Topics in Geophysical Fluid Dynamics: Atmospheric Dynamics, Dynamo Theory, and Climate Dynamics. Springer, New York.
Ghil, M., Kondrashov, D., Lott, F., Robertson, A.W., 2003. Intraseasonal oscillations in the mid-latitudes: observations, theory and GCM results, in: Proceeding of the ECMWF/CLIVAR Workshop on Simulation and Prediction of Intra-Seasonal Variability with Emphasis on the MJO, 3–6 Nov. 2003, ECMWF, Reading, UK. pp. 35–53.
Ghil, M., Mo, K., 1991. Intraseasonal oscillations in the global atmosphere. Part I: Northern hemisphere and tropics. Journal of the Atmospheric Sciences 48, 752–779. doi:10.1175/1520-0469(1991)048<0752:ioitga>2.0.co;2.
Ghil, M., Robertson, A.W., 2000. Solving problems with GCMs: General circulation models and their role in the climate modeling hierarchy, in: Randall, D. (Ed.), General Circulation Model Development: Past, Present and Future. Academic Press, San Diego, pp. 285–325.
Ghil, M., Robertson, A.W., 2002. "waves" vs. "particles" in the atmosphere's phase space: A pathway to long-range forecasting? Proceedings of the National Academy of Sciences 99, 2493–2500. doi:10.1073/pnas.012580899.
Gill, A.E., 1982. Atmosphere-Ocean Dynamics. Academic, New York.
Groth, A., Dumas, P., Ghil, M., Hallegatte, S., 2015. Impacts of natural disasters on a dynamic economy, in: Chavez, M., Ghil, M., Urrutia-Fucugauchi, J. (Eds.), Extreme Events: Observations, Modeling and Economics. American Geophysical Union & Wiley. volume 214 of *Geophysical Monographs*. chapter 19, pp. 343–359.
Groth, A., Feliks, Y., Kondrashov, D., Ghil, M., 2017. Interannual variability in the North Atlantic ocean's temperature field and its association with the wind stress forcing. Journal of Climate 30, 2655–2678. doi:10.1175/jcli-d-16-0370.1.
Groth, A., Ghil, M., 2011. Multivariate singular spectrum analysis and the road to phase synchronization. Physical Review E 84, 036206. doi:10.1103/PhysRevE.84.036206.
Hale, J.K., Verduyn Lunel, S.M., 1993. Introduction to Functional Differential Equations. volume 99 of *Applied Mathematical Sciences*. Springer-Verlag, New York.
Hannachi, A., Straus, D.M., Franzke, C.L.E., Corti, S., Woollings, T., 2017. Low-frequency nonlinearity and regime behavior in the Northern Hemisphere extratropical atmosphere. Reviews of Geophysics doi:10.1002/2015rg000509.
Hansen, A.R., Sutera, A., 1995. The probability density distribution of the planetary-scale atmospheric wave amplitude

revisited. Journal of the Atmospheric Sciences 52, 2463–2472. doi:10.1175/1520-0469(1995)052<2463:tpddot>2.0.co;2.
Hasselmann, K., 1976. Stochastic climate models. I: Theory. Tellus 28, 473–485.
Haurwitz, B., 1940. The motion of atmospheric disturbances on the spherical earth. Journal of Marine Research 3, 254–267.
Held, I.M., 2005. The gap between simulation and understanding in climate modeling. Bulletin of the American Meteorological Society 86, 1609–1614. doi:10.1175/bams-86-11-1609.
Holton, J.R., Haynes, P.H., McIntyre, M.E., Douglass, A.R., Rood, R.B., Pfister, L., 1995. Stratosphere-troposphere exchange. Reviews of Geophysics 33, 403–439. doi:10.1029/95rg02097.
Horel, J.D., 1985. Persistence of the 500 mb height field during Northern Hemisphere winter. Monthly Weather Review 113, 2030–2042. doi:10.1175/1520-0493(1985)113<2030:potmhf>2.0.co;2.
Huth, R., Beck, C., Philipp, A., Demuzere, M., Ustrnul, Z., Cahynová, M., Kyselý, J., Tveito, O.E., 2008. Classifications of atmospheric circulation patterns. Annals of the New York Academy of Sciences 1146, 105–152. doi:10.1196/annals.1446.019.
Itoh, H., Kimoto, M., 1996. Multiple attractors and chaotic itinerancy in a quasigeostrophic model with realistic topography: Implications for weather regimes and low-frequency variability. Journal of the Atmospheric Sciences 53, 2217–2231. doi:10.1175/1520-0469(1996)053<2217:maacii>2.0.co;2.
Itoh, H., Kimoto, M., 1997. Chaotic itinerancy with preferred transition routes appearing in an atmospheric model. Physica D 109, 274–292. doi:10.1016/s0167-2789(97)00064-x.
Jin, F.F., Ghil, M., 1990. Intraseasonal oscillations in the extratropics: Hopf bifurcation and topographic instabilities. Journal of the Atmospheric Sciences 47, 3007–3022. doi:10.1175/1520-0469(1990)047<3007:ioiteh>2.0.co;2.
Jin, F.F., Neelin, J.D., Ghil, M., 1994. El Niño on the devil's staircase: Annual subharmonic steps to chaos. Science 264, 70–72. doi:10.1126/science.264.5155.70.
Kalnay, E., Livezey, R., 1985. Weather predictability beyond a week: an introductory review, in: Ghil, M., Benzi, R., Parisi, G. (Eds.), Turbulence and Predictability in Geophysical Fluid Dynamics and Climate Dynamics, North-Holland, Amsterdam. pp. 311–346.
Kimoto, M., Ghil, M., 1993a. Multiple flow regimes in the northern hemisphere winter. Part I: Methodology and hemispheric regimes. Journal of the Atmospheric Sciences 50, 2625–2644. doi:10.1175/1520-0469(1993)050<2625:mfritn>2.0.co;2.
Kimoto, M., Ghil, M., 1993b. Multiple flow regimes in the northern hemisphere winter. Part II: Sectorial regimes and preferred transitions. Journal of the Atmospheric Sciences 50, 2645–2673. doi:10.1175/1520-0469(1993)050<2645:mfritn>2.0.co;2.
Knutson, T.R., Weickmann, K.M., 1987. 30–60 day atmospheric oscillations: Composite life cycles of convection and circulation anomalies. Monthly Weather Review 115, 1407–1436. doi:10.1175/1520-0493(1987)115<1407:daoclc>2.0.co;2.
Kondrashov, D., Berloff, P., 2015. Stochastic modeling of decadal variability in ocean gyres. Geophysical Research Letters 42, 1543–1553. doi:10.1002/2014GL062871.
Kondrashov, D., Chekroun, M.D., Ghil, M., 2015. Data-driven non-Markovian closure models. Physica D 297, 33–55. doi:10.1016/j.physd.2014.12.005.
Kondrashov, D., Chekroun, M.D., Ghil, M., 2017a. Data-adaptive harmonic decomposition and prediction of Arctic sea ice extent. Submitted.
Kondrashov, D., Chekroun, M.D., Robertson, A.W., Ghil, M., 2013. Low-order stochastic model and "past-noise forecasting" of the Madden-Julian oscillation. Geophysical Research Letters 40, 5305–5310. doi:doi:10.1002/grl.50991.
Kondrashov, D., Chekroun, M.D., Yuan, X., Ghil, M., 2017b. Data-adaptive harmonic decomposition and stochastic modeling of Arctic sea ice, in: A. Tsonis (Ed.), Advances in Nonlinear Geosciences. Springer, pp. 179–205. doi:10.1007/978-3-319-58895-7_10.
Kondrashov, D., Ide, K., Ghil, M., 2004. Weather regimes and preferred transition paths in a three-level quasigeostrophic model. Journal of the Atmospheric Sciences 61, 568–587. doi:10.1175/1520-0469(2004)061<0568:wraptp>2.0.co;2.
Kondrashov, D., Kravtsov, S., Ghil, M., 2006. Empirical mode reduction in a model of extratropical low-frequency variability. Journal of the Atmospheric Sciences 63, 1859–1877. doi:10.1175/jas3719.1.
Kondrashov, D., Kravtsov, S., Ghil, M., 2011. Signatures of nonlinear dynamics in an idealized atmospheric model. Journal of the Atmospheric Sciences 68, 3–12. doi:10.1175/2010jas3524.1.
Kondrashov, D., Kravtsov, S., Robertson, A.W., Ghil, M., 2005. A hierarchy of data-based ENSO models. Journal of Climate 18, 4425–4444. doi:10.1175/jcli3567.1.
Kondrashov, D., Shen, J., Berk, R., D'Andrea, F., Ghil, M., 2007. Predicting weather regime transitions in Northern Hemisphere datasets. Climate Dynamics 29, 535–551. doi:10.1007/s00382-007-0293-2.
Koo, S., Robertson, A.W., Ghil, M., 2002. Multiple regimes and low-frequency oscillations in the Southern Hemisphere's zonal-mean flow. Journal of Geophysical Research: Atmospheres 107, ACL 14–1–13. doi:10.1029/2001jd001353.
Kravtsov, S., Kondrashov, D., Ghil, M., 2005. Multi-level regression modeling of nonlinear processes: Derivation and applications to climatic variability. Journal of Climate 18, 4404–4424. doi:doi:10.1175/JCLI3544.1.
Kravtsov, S., Kondrashov, D., Ghil, M., 2009. Empirical model reduction and the modeling hierarchy in climate dynamics and the geosciences, in: Palmer, T.N., Williams, P. (Eds.), Stochastic Physics and Climate Modeling. Cambridge University Press, pp. 35–72.
Krishnamurthy, V., Achuthavarier, D., 2012. Intraseasonal oscillations of the monsoon circulation over South Asia. Climate Dynamics 38, 2335–2353. doi:10.1007/s00382-011-1153-7.
Krishnamurthy, V., Sharma, A.S., 2017. Predictability at intraseasonal time scale. Geophysical Research Letters 44, 8530–8537. doi:10.1002/2017GL074984.
Kushnir, Y., 1987. Retrograding wintertime low-frequency disturbances over the North Pacific ocean. Journal of the Atmospheric Sciences 44, 2727–2742. doi:10.1175/1520-0469(1987)044<2727:rwlfdo>2.0.co;2.
Legras, B., Ghil, M., 1985. Persistent anomalies, blocking and variations in atmospheric predictability. Journal of the Atmospheric Sciences 42, 433–471. doi:10.1175/1520-0469(1985)042<0433:pabavi>2.0.co;2.

Lindzen, R.S., 1986. Stationary planetary waves, blocking, and interannual variability. Advances in Geophysics 29, 251–273. doi:10.1016/s0065-2687(08)60042-4.
Lindzen, R.S., Farrell, B., Jacqmin, D., 1982. Vacillations due to wave interference: applications to the atmosphere and to annulus experiments. Journal of the Atmospheric Sciences 39, 14–23.
Lott, F., Robertson, A.W., Ghil, M., 2001. Mountain torques and atmospheric oscillations. Geophysical Research Letters 28, 1207–1210. doi:10.1029/2000gl011829.
Lott, F., Robertson, A.W., Ghil, M., 2004a. Mountain torques and Northern Hemisphere low-frequency variability. Part I: Hemispheric aspects. Journal of the Atmospheric Sciences 61, 1259–1271. doi:10.1175/1520-0469(2004)061<1259:mtanhl>2.0.co;2.
Lott, F., Robertson, A.W., Ghil, M., 2004b. Mountain torques and Northern Hemisphere low-frequency variability. Part II: Regional aspects. Journal of the Atmospheric Sciences 61, 1272–1283. doi:10.1175/1520-0469(2004)061<1272:mtanhl>2.0.co;2.
Majda, A.J., Franzke, C.L., Fischer, A., Crommelin, D.T., 2006. Distinct metastable atmospheric regimes despite nearly Gaussian statistics: A paradigm model. Proceedings of the National Academy of Sciences 103, 8309–8314. doi:10.1073/pnas.0602641103.
Majda, A.J., Timofeyev, I., Vanden-Eijnden, E., 1999. Models for stochastic climate prediction. Proceedings of the National Academy of Sciences 96, 14687–14691. doi:10.1073/pnas.96.26.14687.
Marcus, S.L., Ghil, M., Dickey, J.O., 1994. The extratropical 40-day oscillation in the UCLA general circulation model. Part I: Atmospheric angular momentum. Journal of the Atmospheric Sciences 51, 1431–1446. doi:10.1175/1520-0469(1994)051<1431:tedoit>2.0.co;2.
Marcus, S.L., Ghil, M., Dickey, J.O., 1996. The extratropical 40-day oscillation in the UCLA general circulation model. Part II: Spatial structure. Journal of the Atmospheric Sciences 53, 1993–2014. doi:10.1175/1520-0469(1996)053<1993:tedoit>2.0.co;2.
Marshall, J., Molteni, F., 1993. Toward a dynamical understanding of atmospheric weather regimes. Journal of the Atmospheric Sciences 50, 1993–2014.
McWilliams, J.C., 1980. An application of equivalent modons to atmospheric blocking. Dynamics of Atmospheres and Oceans 5, 43–66.
Michelangeli, P.A., Vautard, R., Legras, B., 1995. Weather regimes: Recurrence and quasi stationarity. Journal of the Atmospheric Sciences 52, 1237–1256. doi:10.1175/1520-0469(1995)052<1237:wrraqs>2.0.co;2.
Mitchell, H.L., Derome, J., 1983. Blocking-like solutions of the potential vorticity equation: their stability at equilibrium and growth at resonance. Journal of the Atmospheric Sciences 40, 2522–2536. doi:10.1175/1520-0469(1983)040<2522:blsotp>2.0.co;2.
Mo, K., Ghil, M., 1988. Cluster analysis of multiple planetary flow regimes. Journal of Geophysical Research 93, 10927–10952. doi:10.1029/jd093id09p10927.
Mo, K.C., Ghil, M., 1987. Statistics and dynamics of persistent anomalies. Journal of the Atmospheric Sciences 44, 877–902. doi:10.1175/1520-0469(1987)044<0877:sadopa>2.0.co;2.
Molteni, F., Corti, S., 1998. Long-term fluctuations in the statistical properties of low-frequency variability: Dynamical origin and predictability. Quarterly Journal of the Royal Meteorological Society 124, 495–526. doi:10.1002/qj.49712454607.
Molteni, F., Tibaldi, S., Palmer, T.N., 1990. Regimes in the wintertime circulation over northern extratropics. I: Observational evidence. Quarterly Journal of the Royal Meteorological Society 116, 31–67. doi:10.1256/smsqj.49102.
Moron, V., Robertson, A.W., Qian, J.H., Ghil, M., 2015. Weather types across the Maritime Continent: From the diurnal cycle to interannual variations. Frontiers in Environmental Science , 19 pages,doi:10.3389/fenvs.2014.00065.
Mukougawa, H., 1988. A dynamical model of "quasi-stationary" states in large-scale atmospheric motions. Journal of the Atmospheric Sciences 45, 2868–2888. doi:10.1175/1520-0469(1988)045<2868:admoss>2.0.co;2.
Muñoz, Á., Yang, X., Vecchi, G., W. Robertson, A., Cooke, W., 2017. A weather-type based cross-timescale diagnostic framework for coupled circulation models. Journal of Climate doi:10.1175/jcli-d-17-0115.1.
Namias, J., 1968. Long-range weather forecasting: History, current status and outlook. Bulletin of the American Meteorological Society 49, 438–470.
Neelin, J., Battisti, D., Hirst, A., Jin, F.F., Wakata, Y., Yamagata, T., Zebiak, S., 1998. ENSO theory. Journal of Geophysical Research 104(C7), 14261–14290. doi:10.1029/97jc03424.
Newman, M., Sardeshmukh, P.D., Winkler, C.R., Whitaker, J.S., 2003. A study of subseasonal predictability. Monthly Weather Review 131, 1715–1732. doi:10.1175//2558.1.
Nitsche, G., Wallace, J.M., Kooperberg, C., 1994. Is there evidence of multiple equilibria in planetary wave amplitude statistics? Journal of the Atmospheric Sciences 51, 314–322. doi:10.1175/1520-0469(1994)051<0314:iteome>2.0.co;2.
Palmer, T.N., Williams, P. (Eds.), 2009. Stochastic Physics and Climate Modeling. Cambridge University Press.
Pedlosky, J., 1987. Geophysical fluid dynamics. 2 ed., Springer, New York.
Penland, C., 1989. Random forcing and forecasting using principal oscillation pattern analysis. Monthly Weather Review 117, 2165–2185. doi:10.1175/1520-0493(1989)117<2165:rfafup>2.0.co;2.
Penland, C., 1996. A stochastic model of IndoPacific sea surface temperature anomalies. Physica D 98, 534–558. doi:10.1016/0167-2789(96)00124-8.
Penland, C., Ghil, M., 1993. Forecasting Northern Hemisphere 700-mb geopotential height anomalies using empirical normal modes. Monthly Weather Review 121, 2355–2372. doi:10.1175/1520-0493(1993)121<2355:fnhmgh>2.0.co;2.
Penland, C., Sardeshmukh, P.D., 1995. The optimal growth of tropical sea surface temperature anomalies. Journal of Climate 8, 1999–2024. doi:10.1175/1520-0442(1995)008<1999:togots>2.0.co;2.
Plaut, G., Vautard, R., 1994. Spells of low-frequency oscillations and weather regimes in the Northern Hemisphere. Journal of

the Atmospheric Sciences 51, 210–236. doi:10.1175/1520-0469(1994)051<0210:solfoa>2.0.co;2.
Reinhold, B.B., Pierrehumbert, R.P., 1982. Dynamics of weather regimes: Quasi-stationary waves and blocking. Monthly Weather Review 110, 1105–1145. doi:10.1175/1520-0493(1982)110<1105:dowrqs>2.0.co;2.
Richardson, L.F., 1922. Weather Prediction by Numerical Process. Cambridge University Press, Cambridge, UK.
Rossby, C.G., et al., 1939. Relation between variations in the intensity of the zonal circulation of the atmosphere and the displacements of the semi-permanent centers of action. Journal of Marine Research 2, 38–55.
Sardeshmukh, P.D., Penland, C., 2015. Understanding the distinctively skewed and heavy tailed character of atmospheric and oceanic probability distributions. Chaos 25, 036410. doi:10.1063/1.4914169.
Schneider, S.H., Dickinson, R.E., 1974. Climate modeling. Reviews of Geophysics and Space Physics 25, 447–493.
Silverman, B.W., 1986. Density Estimation for Statistics and Data Analysis. CRC Press.
Smyth, P., Ide, K., Ghil, M., 1999. Multiple regimes in Northern Hemisphere height fields via mixture model clustering. Journal of the Atmospheric Sciences 56, 3704–3723. doi:10.1175/1520-0469(1999)056<3704:mrinhh>2.0.co;2.
Stephenson, D.B., Hannachi, A., O'Neill, A., 2004. On the existence of multiple climate regimes. Quarterly Journal of the Royal Meteorological Society 130, 583–605. doi:10.1256/qj.02.146.
Stinis, P., 2006. A comparative study of two stochastic mode reduction methods. Physica D 213, 197–213. doi:10.1016/j.physd.2005.11.010.
Straus, D.M., Corti, S., Molteni, F., 2007. Circulation regimes: Chaotic variability versus SST-forced predictability. Journal of Climate 20, 2251–2272. doi:10.1175/jcli4070.1.
Straus, D.M., Molteni, F., 2004. Circulation regimes and SST forcing: Results from large GCM ensembles. Journal of Climate 17, 1641–1656. doi:10.1175/1520-0442(2004)017<1641:crasfr>2.0.co;2.
Straus, D.M., Molteni, F., Corti, S., 2017. Atmospheric regimes: The link between weather and the large-scale circulation, in: Franzke, C.L.E., OKane, T.J. (Eds.), Nonlinear and Stochastic Climate Dynamics. Cambridge University Press, pp. 105–135. doi:10.1017/9781316339251.005.
Strong, C., Jin, F.f., Ghil, M., 1995. Intraseasonal oscillations in a barotropic model with annual cycle, and their predictability. Journal of the Atmospheric Sciences 52, 2627–2642. doi:10.1175/1520-0469(1995)052<2627:ioiabm>2.0.co;2.
Strong, C.M., Jin, F.F., Ghil, M., 1993. Intraseasonal variability in a barotropic model with seasonal forcing. Journal of the Atmospheric Sciences 50, 2965–2986. doi:10.1175/1520-0469(1993)050<2965:iviabm>2.0.co;2.
Strounine, K., Kravtsov, S., Kondrashov, D., Ghil, M., 2010. Reduced models of atmospheric low-frequency variability: Parameter estimation and comparative performance. Physica D 239, 145–166. doi:10.1016/j.physd.2009.10.013.
Sura, P., Newman, M., Penland, C., Sardeshmukh, P., 2005. Multiplicative noise and non-gaussianity: A paradigm for atmospheric regimes? Journal of the Atmospheric Sciences 62, 1391–1409. doi:10.1175/jas3408.1.
Tantet, A., van der Burgt, F.R., Dijkstra, H.A., 2015. An early warning indicator for atmospheric blocking events using transfer operators. Chaos 25, 036406. doi:10.1063/1.4908174.
Toth, Z., 1995. Degrees of freedom in Northern Hemisphere circulation data. Tellus A 47, 457–472. doi:10.1034/j.1600-0870.1995.t01-3-00005.x.
Trevisan, A., Buzzi, A., 1980. Stationary response of barotropic weakly non-linear Rossby waves to quasi-resonant orographic forcing. Journal of the Atmospheric Sciences 37, 947–957. doi:{10.1175/1520-0469(1980)037<0947:SROBWN>2.0.CO;2}.
Tziperman, E., Stone, L., Cane, M., Jarosh, H., 1994. El Niño chaos: Overlapping of resonances between the seasonal cycle and the Pacific ocean-atmosphere oscillator. Science 264, 72–74. doi:10.1126/science.264.5155.72.
Vautard, R., 1990. Multiple weather regimes over the North Atlantic: Analysis of precursors and successors. Monthly Weather Review 118, 2056–2081. doi:10.1175/1520-0493(1990)118<2056:mwrotn>2.0.co;2.
Vautard, R., Ghil, M., 1989. Singular spectrum analysis in nonlinear dynamics, with applications to paleoclimatic time series. Physica D 35, 395–424. doi:10.1016/0167-2789(89)90077-8.
Vautard, R., Legras, B., 1988. On the source of midlatitude low-frequency variability. part II: Nonlinear equilibration of weather regimes. Journal of the Atmospheric Sciences 45, 2845–2867. doi:10.1175/1520-0469(1988)045<2845:otsoml>2.0.co;2.
Vautard, R., Mo, K.C., Ghil, M., 1990. Statistical significance test for transition matrices of atmospheric Markov chains. Journal of the Atmospheric Sciences 47, 1926–1931. doi:10.1175/1520-0469(1990)047<1926:sstftm>2.0.co;2.
Vitart, F., 2017. Madden-Julian oscillation prediction and teleconnections in the S2S database. Quarterly Journal of the Royal Meteorological Society 143, 2210–2220. doi:10.1002/qj.3079.
Von Neumann, J., 1955. Some remarks on the problem of forecasting climatic fluctuations, in: Pfeffer, R.L. (Ed.), Dynamics of Climate. Pergamon Press, pp. 9–11. doi:10.1016/b978-1-4831-9890-3.50009-8.
Wallace, J.M., 2000. North Atlantic Oscillation/annular mode: Two paradigms-one phenomenon. Quarterly Journal of the Royal Meteorological Society 126, 791–805. doi:10.1256/smsqj.56401.
Wallace, J.M., Gutzler, D.S., 1981. Teleconnections in the geopotential height field during the Northern Hemisphere winter. Monthly Weather Review 109, 784–812. doi:10.1175/1520-0493(1981)109<0784:titghf>2.0.co;2.
Weickmann, K.M., Lussky, G.R., Kutzbach, J.E., 1985. Intraseasonal (30–60 day) fluctuations of outgoing longwave radiation and 250 mb streamfunction during northern winter. Monthly Weather Review 113, 941–961. doi:10.1175/1520-0493(1985)113<0941:idfool>2.0.co;2.
Zhang, C., Gottschalck, J., Maloney, E.D., Moncrieff, M.W., Vitart, F., Waliser, D.E., Wang, B., Wheeler, M.C., 2013. Cracking the MJO nut. Geophysical Research Letters 40, 1223–1230. doi:10.1002/grl.50244.